https://doi.org/10.5194/essd-2025-388
Preprint. Discussion started: 24 July 2025

Open Access Earth System Science Data Discussions

Mapping the world's coast: a global 100-m coastal typology derived from satellite data using deep learning

Floris R. Calkoen[1,2], Arjen P. Luijendijk[1,2], Susan Hanson[3], Robert J. Nicholls[3,4], Antonio Moreno-Rodenas[1], Hugo de Heer[1,2], and Fedor Baart[5]

[1]Deltares, Boussinesqweg 1, Delft, 2629 HV, Zuid-Holland, The Netherlands
[2]Delft University of Technology, Stevinweg 1, Delft, 2628 CN, Zuid-Holland, The Netherlands
[3]Tyndall Centre for Climate Change Research, University of East Anglia, Norwich, NR4 7TJ, United Kingdom
[4]School of Engineering, University of Southampton, Southampton SO17 1BJ, United Kingdom
[5]Rijkswaterstaat, Ministry of Infrastructure and Water Management, Utrecht, The Netherlands
[1,2]Correspondence to: Floris R. Calkoen (floris.calkoen@deltares.nl)

Abstract. We present a globally consistent, high-resolution (100 m) coastal typology dataset derived from satellite imagery and elevation data using deep learning—the first application of its kind in coastal science. Using a supervised multi-task convolutional neural network, we classified for nearly 10 million coastal transects (one million km of coast) four coastal attributes along the cross-shore profile: (1) sediment type, (2) coastal type, (3) presence/absence of built environment, and (4) presence/absence of human-made coastal defenses. The model, trained on about 1800 globally distributed samples, achieves strong predictive performance with F1 scores ranging from 0.67 to 0.83. Results show that the global coastal sediment distribution consists of 40% sandy, gravel, or shingle; 21% muddy; 13% rocky; and 27% with no sediment. Considering the coastal type, 33% of coasts are cliffed, 22% are sediment plains, 15% are wetlands, and 3% are dune systems (i.e. 26,000 km). Combining sandy, gravel, shingle and muddy sediments, we estimate that 61% of the global coastline consists of soft sediments that are potentially easily erodible. Among sandy, gravel or shingle coasts specifically, 20% are cliff-backed and 16.5% are located on built-up coasts. This global dataset, available in a cloud-optimized format at https://doi.org/10.5281/zenodo.15599096, provides a robust foundation for coastal-change analysis and erosion assessment, and enables new opportunities for broad-scale vulnerability mapping and adaptation planning in the face of accelerating sea-level rise.

1 Introduction

Coastal zones are increasingly under pressure from human development and the cumulative effects of accelerating climate change (Oppenheimer et al., 2019). Urbanization, infrastructure expansion, and land reclamation have transformed coastal landscapes, often leaving limited space for natural processes to unfold (Lansu et al., 2024). As a result, future risks are increasing: erosion and flooding threaten assets, livelihoods and even lives (Barnard et al., 2025), while critical ecosystems face

https://doi.org/10.5194/essd-2025-388
Preprint. Discussion started: 24 July 2025

habitat loss and degradation (European Environment Agency., 2024). Anticipating these risks requires reliable climate data and spatial information to support adaptation planning (Le Cozannet et al., 2017). A coastline's response to drivers such as sea-level rise and increased storminess depends largely on its geomorphology (Stive et al., 2002; Woodroffe, 2002; Masselink, 2014). Yet despite major advances in satellite-based coastal monitoring (Vitousek et al., 2022), no globally consistent, high-resolution coastal typology currently exists to assess vulnerability and ultimately inform sustainable, long-term action.

As early as the 1990s, the potential of geographic information systems to support integrated coastal management was recognized (e.g., Cooper and McLaughlin, 1998). One of the first broad-scale examples was the EUROSION project (Salman et al., 2004), which highlighted coastal erosion risks across Europe and promoted more coordinated shoreline management among EU member states. Its coastal typology provided a structured spatial overview of European coastlines, compiled from national and regional geological datasets. At the global scale, the DIVA (Dynamic Interactive Vulnerability Assessment) model (Vafeidis et al., 2008) introduced a systematic segmentation of the world's coastlines to support sea-level rise impact assessments (e.g., Hinkel et al., 2013; Schuerch et al., 2018). These initiatives show the growing importance of broad-scale coastal typologies for coastal planning but also illustrate the limitations of their time: they relied on heterogeneous national and regional data sources, which led to inconsistencies in classification and variable spatial coverage and quality.

In the last decade, coastal mapping has been rapidly transformed by two key developments: 1) the opening of satellite Earth observation archives (Wulder et al., 2012), which dramatically increased the availability of consistent, high-resolution data across space and time; and 2) the emergence of user-friendly geospatial cloud platforms, which have enabled convenient broad-scale spatial analysis (Gorelick et al., 2017). Together, these advances have enabled global assessments of coastal change at pixel resolution (e.g., Murray et al., 2018) and have established satellite-based coastal monitoring as standard practice in coastal science. Several studies have used these resources for coastal classification: Luijendijk et al. (2018), to focus its shoreline monitoring on sandy coasts; Mao et al. (2022) for broader geomorphological classification; and Hulskamp et al. (2023) to map muddy coasts globally. However, the resulting typologies often remain narrow in scope and rely on traditional tree-based machine learning methods (e.g., Random Forest), which classify each pixel independently. This limits their ability to capture the spatial structures that define many coastal systems — such as dunes, wetlands, tidal inlets, or engineered coasts.

Deep learning (LeCun et al., 2015) offers a more powerful alternative by directly learning spatial patterns from imagery, enabling end-to-end classification of complex, multi-pixel coastal features. Despite its demonstrated success in other Earth observation domains (e.g., Brown et al., 2022), deep learning remains underutilized in coastal science. A few studies (e.g., Dang et al., 2020; Buscombe et al., 2022; Çelik, 2024) have shown its promise, but no global, deep learning-based coastal classification has yet been developed.

Here, we introduce a global coastal typology derived from satellite data using deep learning, developed to support coastal change analysis, erosion assessment, vulnerability mapping, and adaptation planning. The typology adopts a cross-shore perspective, drawing on established classification frameworks that describe coastal systems through interrelated attributes along the land–sea profile (Sharples et al., 2009; Finkl and Makowski, 2020). The dataset comprises nearly 10 million classified transects (Calkoen et al., 2025c)—covering one million kilometers of coastline between 70°S and 70°N—at 100-meter along-shore resolution, and represents the first global-scale application of deep learning in coastal classification. This paper de-

https://doi.org/10.5194/essd-2025-388
Preprint. Discussion started: 24 July 2025

scribes the typology framework, training data, classification model, and resulting dataset, including global summaries and regional comparisons. The typology is distributed in cloud-optimized format, described via a STAC Collection, and archived at: https://doi.org/10.5281/zenodo.15599096.

2 Methods

To produce a globally consistent coastal typology, we designed a scalable classification method built around six components: (1) a classification schema defining the coastal attributes of interest; (2) globally available Earth observation datasets serving as model inputs; (3) a consistent transect grid for systematic sampling; (4) labeled training data for supervised learning; (5) a deep learning model capable of capturing spatial patterns across the cross-shore profile; and (6) an inference workflow for global-scale prediction. The following sections describe the methods used in detail.

2.1 Coastal typology framework

This study adopts a practical coastal classification (Fairbridge, 2004; Finkl, 2004) designed to support coastal monitoring, erosion assessment, vulnerability mapping, and adaptation planning. Conceptually, it builds on cross-shore coastal profiling approaches that classify the coast based on (geomorphological) landform characteristics along the land–sea profile (Sharples et al., 2009; Hanson et al., 2010; French et al., 2016; Finkl and Makowski, 2020). Specifically, we follow the distinction made by Sharples et al. (2009) between shore fabric and coastal landform—corresponding to sediment type and coastal type in our framework—and the related separation of sediment stores and coastal landforms proposed by French et al. (2016), which align with these two attributes respectively. In total, the classification distinguishes four coastal attributes along the cross-shore profile: (1) sediment type, describing the sediment composition near the shoreline; (2) coastal type, characterizing the dominant landform; (3) presence/absence of built environment, and (4) presence/absence of human-made coastal defenses (Fig 2, panel A). The number of classes is intentionally kept limited to enhance interpretability and facilitate global application. The full classification schema is summarized in Table 1.

The sediment type refers to the dominant type in sediment composition of the area just landwards of the immediate shoreline. While drawing on established sediment classification systems—such as Hayes' climatic-sediment framework for the inner continental shelf (Hayes, 1967)—our schema integrates shingle, gravel and sandy shores into one class because these are difficult to reliably distinguish from each other in satellite imagery.

The coastal type refers to the geomorphologically-active, dominant landform found landward of the immediate shoreline. It includes natural landforms with an additional class "engineered structures" for areas where the geomorphology is no longer active due to human influences. Sediment plains describe low-lying terrain composed of mostly unconsolidated materials and are commonly found in deltaic environments. In contrast, bedrock plains are also low-lying areas, but then composed of mostly solid rock, often appearing in uplifted regions with resistant lithologies, such as the granitic coasts of the Nordic countries. Cliffs are defined by their elevation and steep gradients, generally exceeding 15 m in height, with typical slopes higher than 30 degrees. Wetland coasts include all three major muddy classes, encompassing salt marshes, mangroves, and sabkha systems.

In addition, the schema includes a transitional class for moderately sloped coasts, where land rises gradually from sea to higher hinterland, a landform that is found in Northern Spain and Ireland. The coastal types are classified taking into account anthropogenic modification. For example, when dunes have been flattened due to urban expansion, the area is categorized as a sediment plain. This applies for example to coastal segments in the Basque region (Spain), where former dune systems, like Zarautz, have been largely urbanized. Similarly, polder landscapes in the Netherlands, which represent areas of reclaimed land, are categorized as sediment plains with defense when they include visible flood protection infrastructure, such as a dike. Areas where natural landform is no longer active due human influences, such as port areas, are categorized under “engineered structures”.

The final two attributes in coastal typology act as binary modifiers. The built environment field indicates whether an area is predominantly developed or urbanized. Similarly, the “has defense” attribute specifies the presence of visible hard-engineering structures designed to protect against coastal erosion or flooding.

2.2 Collecting training data

The training data for the supervised classification was collected using a custom web application. A total of approximately 1800 training samples were provided by more than 15 experts, with the vast majority (98%) coming from the authors of this paper. As with any supervised learning framework, the quality and character of the classification depend strongly on the underlying training data. In this study, approximately 95% of samples were labeled by the lead author. As a result, the training data, and by extension the resulting typology, reflect the interpretation and domain understanding of that individual. Appendix D1 shows the global distribution of training samples. While the training dataset covers a broad geographic range, including samples from coastlines around the world, most are concentrated along European coasts.

Each sample was classified based on an area of interest measuring 400 m alongshore by 2 km cross-shore (Fig 2, panel B), defined along a transect from the Global Coastal Transect System (GCTS)(Calkoen et al., 2025c). Experts viewed this area on ESRI World Imagery (2.5 m resolution) and assigned labels for each of the four classification tasks: sediment type, coastal type, presence/absence of built environment and presence/absence of human-made coastal defenses. The interface also provides direct links to Google Street View, which users relied on when classes could not be confidently assigned from experience and/or the top-down imagery alone. Labels were assigned to the best of the contributors’ ability using these high-resolution sources, even though they were aware that the model would be trained on lower-resolution Sentinel-2 imagery (10 m). Class balance across all four tasks was difficult to maintain, but the overall data collection process aimed for class balance in coastal type, resulting in more even representation for that attribute (Tab. 3). We refer to this training dataset as CoastBench (Calkoen et al., 2025a): A global training dataset for coastal classification using satellite imagery and elevation data. It is publicly available, described in a STAC Collection, released under a CC-BY-4.0 license, and accessible at https://doi.org/10.5281/zenodo.15800284, with new samples welcome via the web application.

https://doi.org/10.5194/essd-2025-388
Preprint. Discussion started: 24 July 2025

Open Access Earth System Science Data Discussions

Table 1. Classification schema used in the coastal typology model, including class definitions and number of training samples.

Attribute	Class name	Description
Sediment type	Sandy, gravel or small boulder sediments	Shorelines composed of unconsolidated materials such as sand, gravel, shingles, and small boulders (0.0652 to 512 mm in diameter).
	Muddy sediments	Shorelines dominated by fine-grained sediments like silt and clay, forming environments such as mudflats and tidal flats.
	Rocky shore platform or large boulders	Shorelines composed of solid rock formations, including shore platforms or large boulders greater than 512 mm in diameter.
	No sediment or shore platform	Shorelines with minimal visible sediment, typically around rocky cliffs, steep faces, or human-made structures such as sea walls.
Coastal type	Cliffed or steep	Coastal areas with cliffs or steep rock faces, generally exceeding 15 m, with slopes of 30 degrees or greater.
	Moderately sloped	Coastal areas with gentle to moderate slopes (<30 degrees), often composed of unconsolidated sediment or soft rock.
	Bedrock plain	Low-lying coastal areas (<15m) primarily formed by consolidated bedrock, including skerries, with minimal variability in elevation .
	Sediment plain	Low-lying coastal areas (<15m) with flat or gently sloping unconsolidated sediment, often featuring beach ridges or washover complexes.
	Dune	Sandy coastal areas characterized by wind-formed dunes, often stabilized by vegetation such as grasses.
	Wetland	Coastal areas periodically flooded, including environments such as tidal flats, salt marshes, mangroves, sabkhas, and peatlands.
	Inlet	A narrow coastal waterway where the sea meets the land creating dynamic systems such as estuaries and lagoons.
	Engineered structures	Coastal areas dominated by engineered structures such as port areas, sea walls, breakwaters and groynes, where the natural coastal landscape is obscured or heavily modified.
Is built environment	True	The coastal area is characterized predominantly by human-made structures, including buildings, industrial complexes, and port facilities.
	False	The coastal area remains largely natural, with minimal or no presence of built structures like buildings, industrial zones, or ports.
Has defense	True	Visible hard engineering structures, designed to protect against coastal erosion and flooding (e.g., sea walls, breakwaters), are present.
	False	No visible hard engineering structure, designed to protect against coastal erosion and flooding (e.g., sea walls, breakwaters), are present.

https://doi.org/10.5194/essd-2025-388
Preprint. Discussion started: 24 July 2025

Open Access Earth System Science Data Discussions

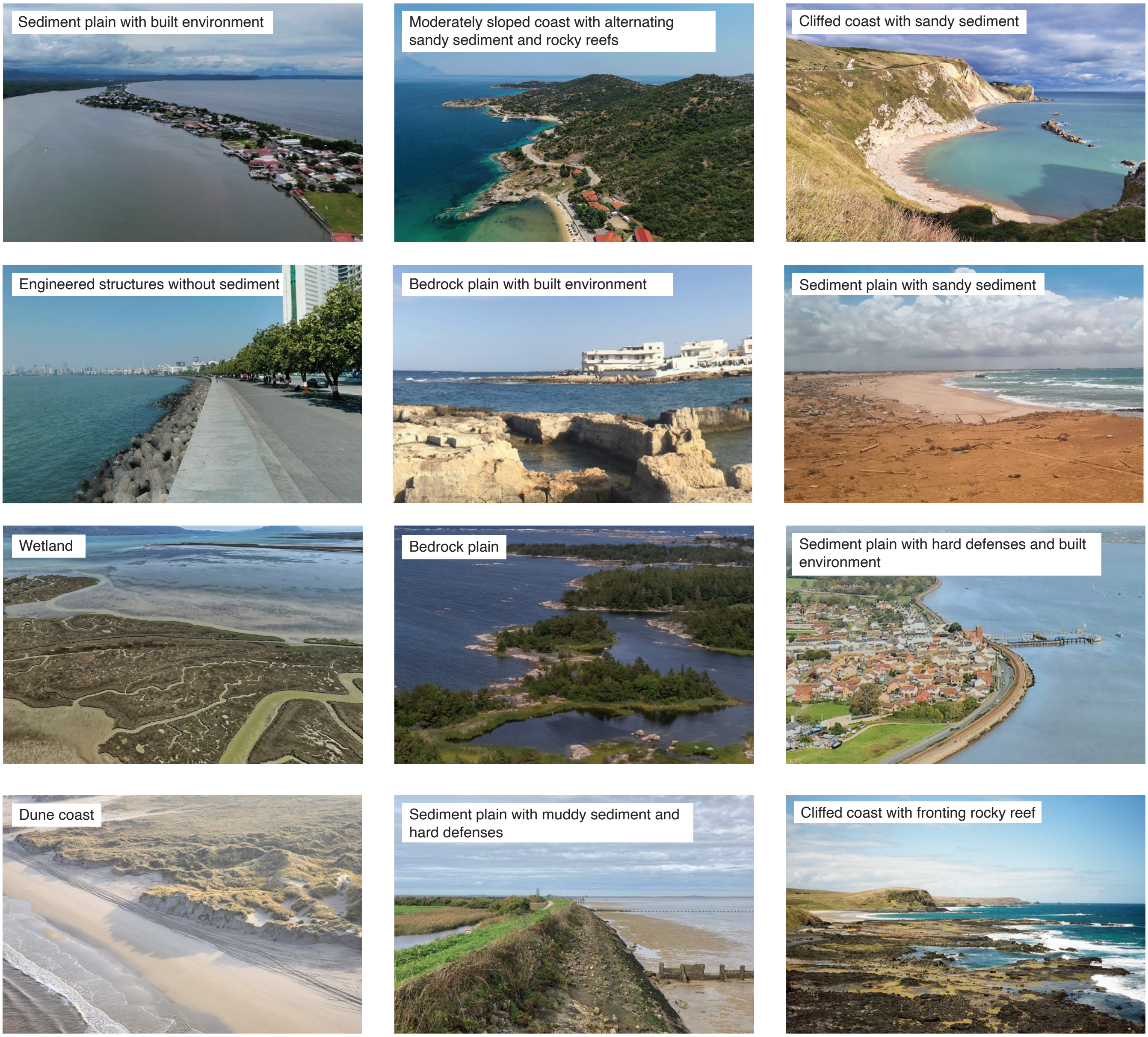

Figure 1. Illustrative examples of coastal environments, showing variations in sediment type, coastal type, presence of built environments, and coastal defense structures. The images were contributed by the authors and sourced from publicly available imagery.

https://doi.org/10.5194/essd-2025-388
Preprint. Discussion started: 24 July 2025

Open Access Earth System Science Data Discussions

2.3 Satellite data acquisition

This study integrates multi-source Earth observation data to construct a standardized coastal typology datacube with 15 feature maps (Fig. 2, panel C). The datacube is constructed in two main stages: (1) generation of an annual cloud-free Sentinel-2 composite, and (2) fusion of this composite with elevation layers and derived spatial features to create the final 15-channel input stack. The input stack combines the cloud-free Sentinel-2 composite—capturing optical and infrared reflectance—with elevation data from the Copernicus DEM (European Space Agency (ESA), 2019) and the coastal DeltaDTM dataset (Pronk et al., 2024). Both Copernicus DEM and DeltaDTM were used because DeltaDTM offers higher accuracy for coastal areas but is limited to elevations below 30 m, whereas Copernicus DEM provides coverage extending beyond this elevation. The flow chart (Panel D) in figure 2 shows the data processing steps. All datasets were accessed via STAC APIs: Sentinel-2 and Copernicus DEM through the Microsoft Planetary Computer, and DeltaDTM via the CoCliCo catalog. Inputs were reprojected to a common 10 m UTM grid using bicubic interpolation and normalized to the [0, 1] range to ensure consistent model input scaling.

The classification was performed on standardized image chips of 2.8 km $\times$ 2.8 km (approximately 8 km^2), each centered on a coastal transect from GCTS (Calkoen et al., 2025c). A region of interest, defined as a 400 m alongshore by 2000 m cross-shore rectangle, anchors the target classification zone within each chip, while the surrounding area provides spatial context for the model. This is illustrated in figure 2 (Panel C), where the outer red box indicates the complete image chip, and the inner orange box marks the model's target area.

2.3.1 Sentinel-2 composites

An annual, cloud-free Sentinel-2 composite was generated for the period 2023-01-01 to 2024-01-01. Imagery was retrieved via the Microsoft Planetary Computer STAC catalog and processed per MGRS tile. To ensure balanced spatial and temporal sampling, scenes were grouped by orbital- track and partitioned into four synthetic groups, while enforcing a five-day minimum interval and selecting the least cloudy scene per period. Cloud and shadow masking used the Sentinel-2 Scene Classification Layer (SCL), excluding pixels labeled as “no data”, “dark area pixels”, or “clouds high probability”. A median composite was computed from remaining pixels, resulting in a, cloud-free, composite image per tile. The final composite includes six reflectance bands—blue, green, red, NIR, SWIR16, and SWIR22—resampled to a unified 10 m UTM grid using bicubic interpolation. The resulting global, cloud- and ice free composite was cataloged as a STAC collection for downstream interoperability.

2.3.2 Coastal typology cube

The coastal typology cube was constructed by combining the annual Sentinel-2 composite with elevation data from the Copernicus DEM and the DeltaDTM product, all resampled to a common 10 m UTM grid. In addition to the six Sentinel-2 reflectance bands and two elevation layers, the cube includes four spectral indices (NDVI, NDWI, MNDWI, NDMI) and a relative elevation layer capturing local terrain contrast. Spatial context is encoded through binary masks for the region of interest (ROI), as

https://doi.org/10.5194/essd-2025-388
Preprint. Discussion started: 24 July 2025

Open Access Earth System Science Data Discussions

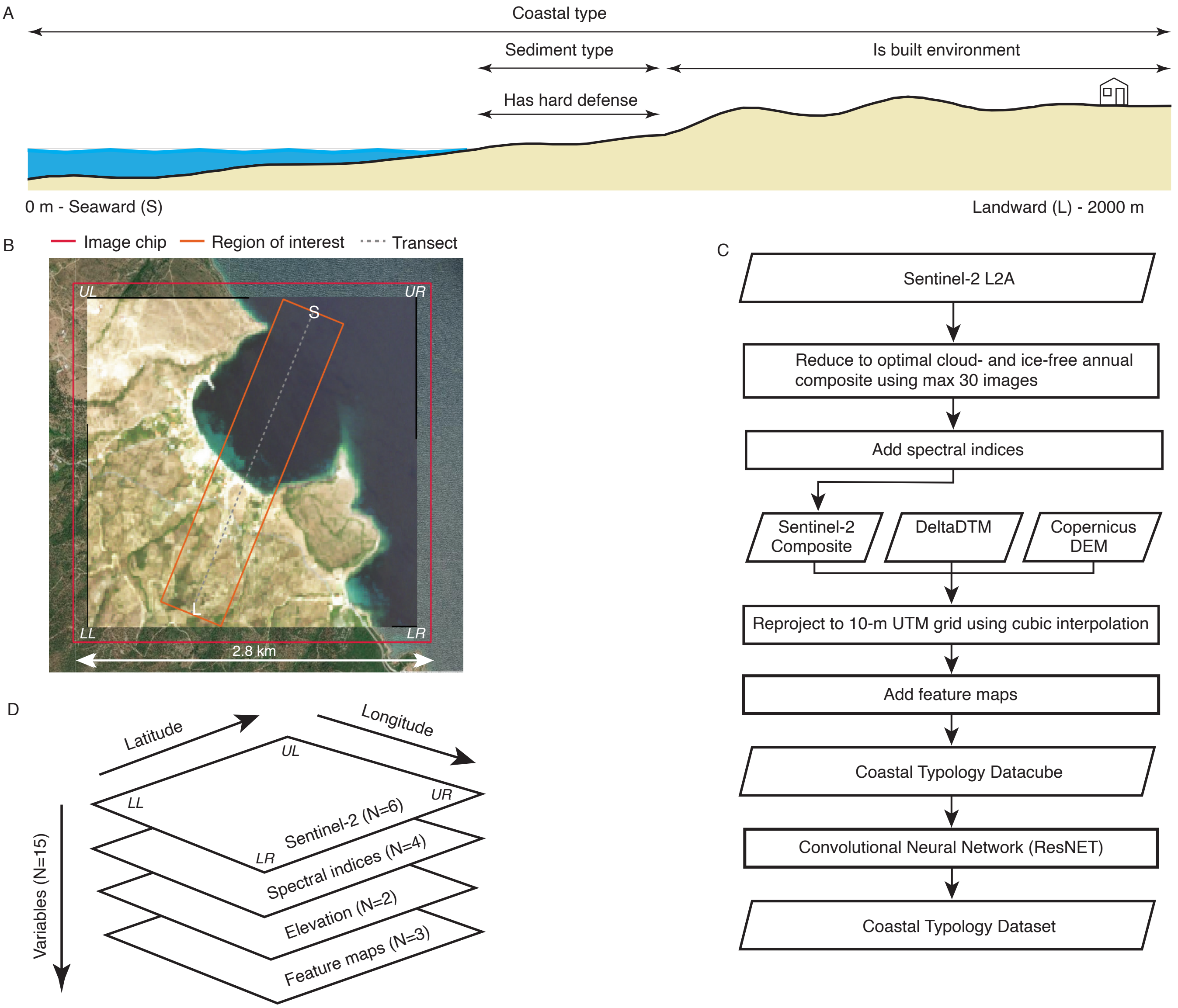

Figure 2. Overview of the coastal typology classification workflow. **(A)** Conceptual cross-shore model describing the classification framework, which distinguishes four coastal attributes along the sea–land profile: sediment type, coastal type, whether the area is predominantly built-up, and presence of coastal defenses. **(B)** Illustration of the image sampling process. Each chip (2.8 km × 2.8 km) is centered on a GCTS coastal transect (dashed gray line); the region of interest (orange rectangle) defines the target area for classification, while the surrounding red area provides additional context to the model. The basemap is from Esri World Imagery. **(C)** Flow chart of the data processing and classification pipeline, from raw Sentinel-2 imagery and elevation data to classified coastal attributes. **(D)** Schematic of the Coastal Typology Cube, consisting of 15 variables: 6 Sentinel-2 bands, 4 spectral indices, 2 elevation layers, and 3 spatial feature maps.

https://doi.org/10.5194/essd-2025-388
Preprint. Discussion started: 24 July 2025

well as landward and seaward points of the respective transect. Thus we obtain a coastal typology cube with 15 maps per image chip, normalized to the [0,1] range using robust min-max scaling with the values specified in Table2, which also summarizes the resulting input stack used for classification.

Table 2. Model input variables used in the coastal typology data cube. Each variable is listed with its source, feature transformation (if any), normalization method, and robust clip range. Robust Min-Max scaling was applied using the values provided in the Clip Range column. Variables marked with an asterisk are derived from source data.

Variable	Source	Description	Scaling	Clip Range
blue	Sentinel-2	Surface reflectance (B2)	Robust Min-Max	[1000, 4000]
green	Sentinel-2	Surface reflectance (B3)	Robust Min-Max	[1100, 4300]
red	Sentinel-2	Surface reflectance (B4)	Robust Min-Max	[1000, 5000]
nir	Sentinel-2	Near-infrared reflectance (B8)	Robust Min-Max	[1000, 6500]
swir16	Sentinel-2	Shortwave infrared reflectance (B11)	Robust Min-Max	[1000, 6000]
swir22	Sentinel-2	Shortwave infrared reflectance (B12)	Robust Min-Max	[1000, 5500]
NDVI	Sentinel-2*	Normalized Difference Vegetation Index	Robust Min-Max	[-0.25, 0.50]
NDWI	Sentinel-2*	Normalized Difference Water Index	Robust Min-Max	[-0.60, 0.30]
MNDWI	Sentinel-2*	Modified NDWI (green–SWIR)	Robust Min-Max	[-0.45, 0.45]
NDMI	Sentinel-2*	Normalized Difference Moisture Index	Robust Min-Max	[-0.25, 0.45]
cop_dem_glo_30	Copernicus DEM	Absolute elevation (m)	Robust Min-Max	[-20, 150]
deltadtm	DeltaDTM	Absolute elevation (m)	Robust Min-Max	[-20, 30]
cop_dem_glo_30_rel	Copernicus DEM*	Relative elevation (local min/max)	Robust Min-Max	[0, 75]
deltadtm_rel	DeltaDTM*	Relative elevation (local min/max)	Robust Min-Max	[0, 30]
region_of_interest_mask	GCTS*	Binary mask for 400 m $\times$ 2000 m region of interest	—	—
landward_mask	GCTS*	Binary mask for landward side of transect	—	—
seaward_mask	GCTS*	Binary mask for seaward side of transect	—	—

2.4 Deep learning classification model

The classification task is a multi-task, multi-class problem (Ruder, 2017), where the model predicts four coastal attributes across the water-land cross-shore profile per image: two multi-class labels (*sediment type* and *coastal type*) and two binary labels (*has defense* and *is built environment*). All tasks are trained jointly using a shared deep learning model based on a ResNet-50 (He et al., 2016) backbone pretrained on ImageNet. The backbone is followed by four parallel classification heads, each producing task-specific predictions from a shared feature representation. Model input consists of 15 channels (the coastal typology cube), including Sentinel-2 reflectance bands, spectral indices, elevation layers, and region-of-interest masks, normalized using robust min-max scaling (see Table 2).

To balance task contributions, the total loss was defined as a weighted sum of task-specific loss functions. Multi-class outputs were optimized using categorical cross-entropy, and binary outputs using binary cross-entropy with logits. Loss scaling was

https://doi.org/10.5194/essd-2025-388
Preprint. Discussion started: 24 July 2025

Open Access Earth System Science Data Discussions

set to 1.0 for *sediment type* and *coastal type*, and 0.5 for *has defense* and *is built environment*, prioritizing the more complex typological classes while preserving sensitivity to binary classifications.

The model was implemented in PyTorch Lightning, with experiment tracking and checkpointing managed via Weights & Biases (WandB). A hyperparameter sweep explored learning rate, batch size, and loss scaling factors. Data was split into training, validation, and test sets (70:15:15), while ensuring no spatial overlap between splits. Data augmentation during training included random flips, rotations and affine transformations.

2.5 Validation

Model performance is evaluated over 10 independent training runs, each initialized with a different random seed, using a fixed 70:15:15 train–validation–test split. To avoid data leakage, overlapping image chips are assigned exclusively to a single partition. All metrics are computed on the held-out test set and reported (Tab. 3) as the mean with standard deviation across the 10 runs. Evaluation focuses on the per-class F1-score as the primary performance metric, due to its robustness to class imbalance compared to accuracy (Christen et al., 2023). Task-level performance is summarized using the macro-F1 metric, defined as the unweighted mean of per-class F1-scores: $\text{Macro-F1} = \frac{1}{N}\sum_{i=1}^{N}\text{F1}_i$, where N is the number of classes and F1_i is the F1-score for class i.

As shown in Table 3, the model achieves its highest macro-F1 scores on the binary classification tasks: *is built environment* (0.83 $\pm$ 0.02) and *has defense* (0.77 $\pm$ 0.04), both supported by large and training sets (e.g., $N = 1177$ for the negative class in *has defense*). Intermediate performance is observed for the four-class *sediment type* task (0.76 $\pm$ 0.04), while the eight-class *coastal type* task yields the lowest macro-F1 (0.67 $\pm$ 0.01), consistent with its higher class complexity and smaller sample sizes. A general, though not strict, relationship between training sample size and performance is evident. Lower F1-scores are recorded for rare classes such as “Inlet” (0.61 $\pm$ 0.12, $N = 139$) and “Dune” (0.65 $\pm$ 0.08, $N = 156$). However, strong performance is still achieved by some underrepresented classes, including “Muddy sediments” (0.86 $\pm$ 0.04, $N = 242$) and “Wetland” (0.77 $\pm$ 0.08, $N = 150$), suggesting that spectral distinctiveness or consistent labeling may offset the impact of limited sample size. Standard deviations across runs are generally low (≤ 0.12), indicating stable performance. Notable exceptions include “Engineered structures” and “Inlet”, which exhibit higher variance and may reflect label ambiguity or sampling sensitivity. The “Moderately sloped” class proves particularly challenging (F1 = 0.55 $\pm$ 0.08, $N = 209$), likely due to geophysical ambiguity and class overlap with “Dune” and “Cliffed or steep”.

2.6 Inference at scale

For large-scale inference, the final model was retrained on the full dataset, utilizing an 85:15 train-validation split during this phase to maximize training coverage while still having an independent validation partition for early stopping to prevent overfitting. Inference was performed by dynamically constructing coastal typology cubes using the STAC API processing per coastal grid tile (Calkoen et al., 2025c). Tiles were processed using a coastal grid at zoom level 9. Distributed inference was executed on a SLURM cluster using Dask JobQueue, with each worker allocated 32 GB of memory and four threads. Batches

https://doi.org/10.5194/essd-2025-388
Preprint. Discussion started: 24 July 2025

Table 3. Per-class F1-scores (mean ± standard deviation) for each classification task: Sediment type (4 classes), Coastal Type (8 classes), Is Built Environment (True/False), and Has Defense (True/False). Each score represents the average performance over 10 model runs. The final row reports the macro-F1 score for each task, computed as the unweighted mean across classes. The final column shows the overall average across all tasks. N refers to the number of samples in the training data. Empty cells indicate that a given class is not defined for that task.

Class	N	sediment type	Coastal Type	Is Built Environment	Has Defense	Average
No sediment or shore platform	343	0.70 ± 0.07				
Sandy gravel or small boulder sediments	745	0.84 ± 0.04				
Muddy sediments	242	0.86 ± 0.04				
Rocky shore platform or large boulders	305	0.64 ± 0.09				
Bedrock plain	153		0.62 ± 0.07			
Cliffed or steep	334		0.78 ± 0.06			
Dune	156		0.65 ± 0.08			
Engineered structures	146		0.69 ± 0.11			
Inlet	139		0.61 ± 0.12			
Moderately sloped	209		0.55 ± 0.08			
Sediment plain	348		0.68 ± 0.07			
Wetland	150		0.77 ± 0.08			
False	977 / 1177			0.86 ± 0.02	0.88 ± 0.02	
True	658 / 458			0.79 ± 0.03	0.66 ± 0.07	
Macro F1	–	0.76 ± 0.04	0.67 ± 0.03	0.83 ± 0.02	0.77 ± 0.04	**0.76 ± 0.03**

were sized at approximately twice the number of active workers to optimize asynchronous requests, throughput and overall resource utilization.

2.7 Software

This study used the Pangeo ecosystem (Hamman et al., 2018) and the OpenDataCube (ODC) (Killough, 2018) framework, which together provide a scalable foundation for accessing, transforming, and analyzing large-scale geospatial raster data. Raster retrieval is managed via `ODC-STAC`, while `ODC-GEO` and its geobox model are used extensively for spatial operations such as reprojection and clipping. Distributed data processing and inference are performed using `Dask 2025.2.0` (Rocklin, 2015), enabling parallel, lazy execution across a SLURM cluster. Deep learning routines are implemented in `PyTorch Lightning 2.5`, with `PyTorch 2.2` (Paszke et al., 2019) providing GPU-accelerated training and Weights & Biases (Biewald, 2020) used for experiment tracking. All computations were performed using `Python 3.12`, and the code—including data models and deep learning architectures—is available through the open-source `CoastPy` (Calkoen et al., 2025c) package. Geospatial analytics are conducted primarily using `DuckDB 1.2` (Raasveldt and Mühleisen, 2019), including its spatial extension and H3 bindings for hexagonal hierarchical spatial aggregation.

https://doi.org/10.5194/essd-2025-388
Preprint. Discussion started: 24 July 2025

Open Access Earth System Science Data Discussions

3 Results

We present a globally consistent coastal typology dataset based on the classification of nearly 10 million GCTS transects, covering close to one million kilometers of coastline between 70°S and 70°N, at 100 m alongshore resolution. The following sections describe the spatial distribution of predicted classes at global (Section 3.1) and continental scale (Section 3.2), provide a local example to illustrate prediction detail (Section 3.3) and examine typological relationships across tasks (Section 3.4). The section concludes by outlining the structure and accessibility of the released dataset (Section 3.5).

3.1 A Global Coastal Typology

Figures 3 and 4 present global maps of predicted *sediment type* and *coastal type*, each aggregated to a level-3 H3 hexagonal grid using the most frequent class (mode) per cell. These coarser summaries, based on nearly 10 million classified coastal transects, reveal broad-scale patterns in sediment type and geomorphology. More regional European maps are included in appendix B1 and B1. Similar spatial summaries of the binary attributes *is built environment* and *has defense* are provided in appendix A1 and A2.

Sandy coasts dominate along much of Africa, Southeast Asia, and Australia, while muddy shorelines concentrate in tropical deltas and back-barrier systems such as the Gulf of Guinea (Fig. 4) and the Wadden Sea (App. B1). Rocky shore platforms appear in more localized areas (e.g., western Ireland; App. B1), while high-latitude coasts in Norway, Alaska, and southern Chile are frequently classified as “no sediment or shore platform”. Considering *coastal type* map, cliffs dominate in tectonically active or glaciated regions (e.g., Nordic countries; Kamchatka, Russia; and, Southern Chile), wetlands cluster in low-lying tropical zones (e.g., Bangladesh, West Africa), and dune systems are found along the coasts of North Brazil and southwestern France (App. B2). Engineered structures are concentrated in highly urbanized or industrialized coasts such as Japan, eastern China, and the San Francisco Bay Area.

3.2 A quantitative global and continental overview

Table 4 provides a quantitative overview of typological coverage by class and continent. Among sediment types, sandy coasts are the most common globally (40%), with particularly high representation in Africa (65%). Muddy shores account for 21% of the global length and are more prevalent in Asia (29%) and Africa (22%), typically reflecting tropical deltas and estuarine systems. Rocky shore platforms—characterized by large boulders or exposed rock—make up 13% and are relatively evenly distributed across continents. The class “No sediment or shore platform” represents 27% of the global coast and is concentrated in high-latitude, high-relief regions such as Europe (36%), North America (37%), and South America (35%), corresponding to the cliff-dominated settings highlighted in Section 3.1 (Fig. 4).

For coastal types, cliffed or steep coasts are the most frequent globally (33%), most prominent in Europe, North America, and South America. Sediment plains (22%) and wetlands (15%) are more common in Asia and Africa, reflecting the prevalence of low-lying humid coasts. Dune systems are relatively rare (3% globally), but appear more prominently in Africa (10%), often along straight, sediment-rich coasts such as southwestern France (Aquitaine) (App. B2). Engineered structures make

https://doi.org/10.5194/essd-2025-388
Preprint. Discussion started: 24 July 2025

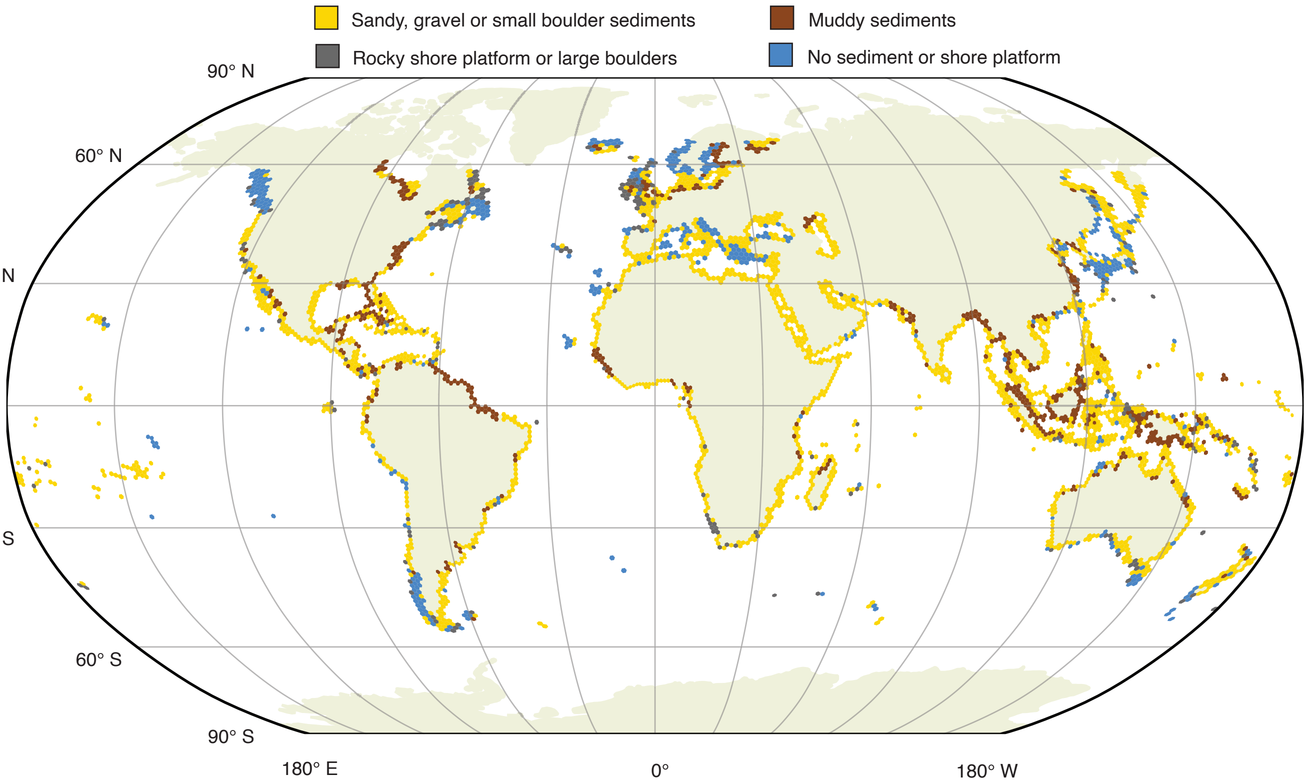

Figure 3. Global map of predicted *sediment type*, aggregated on a level-3 H3 hexagonal grid using majority class (mode) per cell. This coarser view summarizes almost 10 million classified coastal transects, highlighting regional patterns. Basemap: Natural Earth.

up a modest share (3%), with the highest in Asia (7%) and Europe (5%), consistent with the high density of urbanized and industrialized coastlines in these regions.

The global coastline remains predominantly natural: 87% of segments are not classified as built environment, and 91% show no coastal defense structures, with maps provided in appendix A1 and A2. However, regional contrasts are notable. Asia stands out with 21% of its coastline classified as built and 17% showing defense infrastructure, followed by Europe (18% built, 11% defended). In contrast, Africa, Oceania, and South America remain largely undeveloped, with built and defended segments typically below 6%. Overall, the data show that 59% of built-up coastlines also contain coastal defenses. Conversely, and as expected, the vast majority (83%) of defended coasts are situated along built-up areas.

The class distributions are also computed at the country level. Appendix C1 shows normalized class percentages per country for all four classification tasks using a stacked bar plot, enabling visual comparison of coastal typology across national boundaries. A full tabular summary of these country-level statistics is also provided in the Zenodo archive (Sec. 3.5), offering both absolute (km) and relative (%) values for each class and classification task.

https://doi.org/10.5194/essd-2025-388
Preprint. Discussion started: 24 July 2025

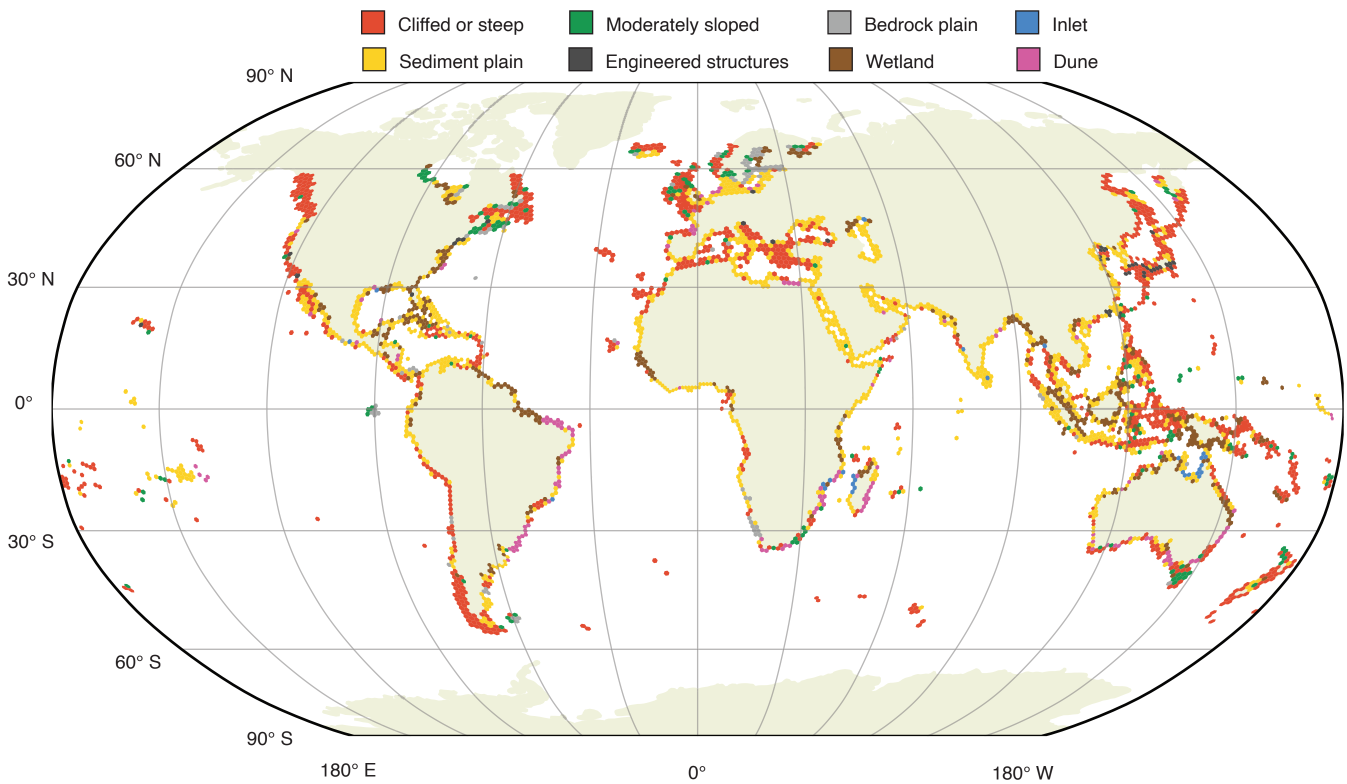

Figure 4. Global map of predicted *coastal types*, aggregated on a level-3 H3 grid using the most frequent class (mode) per cell. This coarser view summarizes almost 10 million classified coastal transects, highlighting regional patterns. Basemap: Natural Earth.

3.3 Local-Scale Example: Saunton Sands

Figure 5 presents detailed predictions near Saunton Sands, a geomorphologically diverse stretch of coastline in southwest England. This area includes a range of sediment types, landforms, and anthropogenic features, offering a representative setting to illustrate specifically the resolution at which the global coast is mapped.

North of the estuary, the model correctly identifies a well-developed dune system (Fig. 5, Panel A). South of the estuary, where dune forms are absent and a low embankment is present (Fig. 5, Panel B), the classification as “sediment plain” is appropriate. Within the estuary, sandy tidal flats are mapped as “sandy, gravel or small boulder” sediment type, with adjacent low-relief terrain labeled as “moderately sloped” coastal type (Fig. 5, Panel C). Built-up settlements along the estuary are also captured. Further upstream, the model successfully tracks the transition to muddy sediments.

At Croyde (Fig. 5, Panel D), the pocket beach is classified as “sandy, gravel or small boulder sediments” without defenses, and its hinterland is labeled “moderately sloped”. A “dune” classification could also be argued for this coastal type and this is probably an example that relates to the relatively lower performance scores of these classes (Tab. 3). Just north of Croyde, the model detects the shift to a rocky reef and correctly assigns the “cliffed or steep” coastal type.

https://doi.org/10.5194/essd-2025-388
Preprint. Discussion started: 24 July 2025

Table 4. Global and continent-wise summary of coastal typology classes per task, by total coastal length (10^3 km) and relative proportion (%). Abbreviations: Global (GL), Europe (EU), Asia (AS), Africa (AF), North America (NA), South America (SA), Oceania (OC), Antarctica (AN).

		Length (10^3 km)								Percentage (%)							
Attribute	**Class**	**GL**	**EU**	**AS**	**AF**	**NA**	**SA**	**OC**	**AN**	**GL**	**EU**	**AS**	**AF**	**NA**	**SA**	**OC**	**AN**
Sediment type	Sandy gravel or small boulder sediments	374	61	96	35	102	31	46	2	40	35	46	65	34	32	48	49
	Muddy sediments	193	27	62	12	50	19	23	0	21	15	29	22	17	19	25	1
	Rocky shore platform or large boulders	119	25	25	5	37	13	14	1	13	14	12	8	12	13	14	16
	No sediment or shore platform	252	64	27	3	109	34	12	1	27	36	13	5	37	35	13	33
Coastal Type	Cliffed or steep	306	65	47	8	113	44	26	3	33	36	22	14	38	45	28	60
	Moderately sloped	125	31	21	3	42	14	13	1	13	17	10	6	14	14	14	29
	Bedrock plain	74	20	8	3	32	6	5	0	8	11	4	5	11	6	5	5
	Sediment plain	206	32	67	21	52	13	21	0	22	18	32	40	17	13	22	3
	Dune	26	4	4	5	4	3	6	0	3	2	2	10	1	3	6	1
	Wetland	143	16	45	11	37	16	18	0	15	9	21	20	13	16	19	1
	Inlet	25	2	5	2	10	1	5	0	3	1	2	4	3	1	5	0
	Engineered structures	33	8	14	1	8	1	1	0	3	5	7	1	3	1	1	2
Is Built Environment	False	816	146	166	51	267	92	90	4	87	82	79	94	89	94	95	96
	True	122	32	44	3	32	6	5	0	13	18	21	6	11	6	5	4
Has Defense	False	852	158	174	52	277	94	92	4	91	89	83	97	93	97	97	98
	True	86	20	36	2	22	3	3	0	9	11	17	3	7	3	3	2

Further south, near Westward Ho(Fig. 5, Panel B), the model identifies the transition to a heavily modified shoreline, assigning both *is built environment* and *has defense*. Beyond this area, predictions capture a return to natural cliffed coastline without defenses. Across the full extent, the outputs show spatial coherence, reflect smooth transitions between class boundaries, and align well with observed landforms and infrastructure.

3.4 Co-occurrence and typological relationships

To explore relationships across the four classification dimensions, we present two complementary visualizations: normalized co-occurrence matrices between *sediment type* and *coastal type* (Figure 6), and a multi-level Sankey diagram showing co-distribution patterns across all tasks (Fig. 7). The co-occurrence matrices express conditional relationships, with each row representing a single class and columns showing the relative composition of paired classes, normalized to 100%. The Sankey diagram extends this by visualizing how class transitions unfold across all four tasks. Each vertical layer represents one classification dimension, and flow thickness corresponds to the total coastline length (in kilometers) shared by the connected classes.

Several patterns in these visualizations align with well-known coastal geomorphologies. Wetlands co-occur almost exclusively with muddy sediment shorelines (96%; Figure 6b), and dune coasts are paired with sandy shorelines (98%). Cliffed or steep coasts are most frequently associated with the absence of visible sediment (54%), but also co-occur with rocky platforms

https://doi.org/10.5194/essd-2025-388
Preprint. Discussion started: 24 July 2025

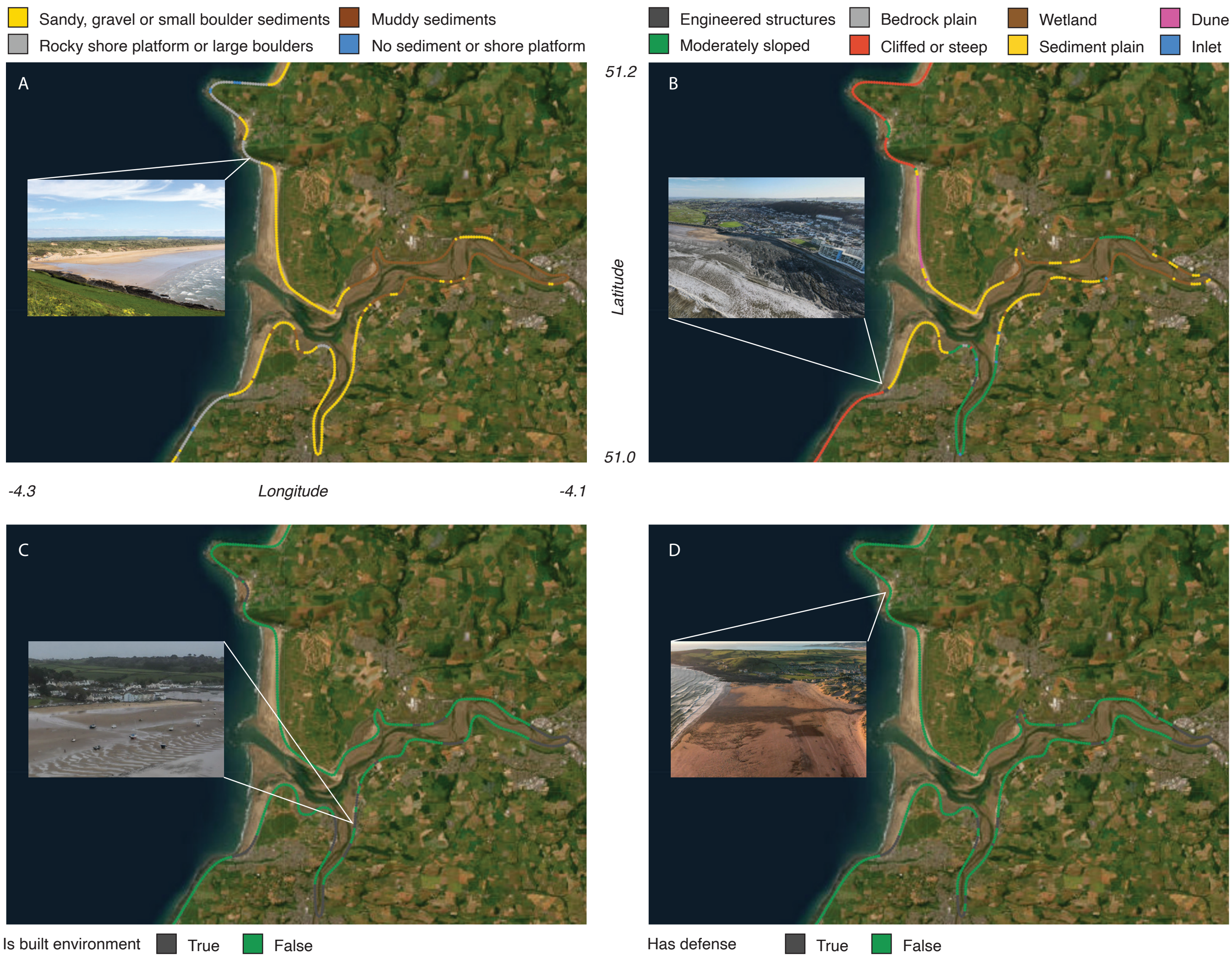

Figure 5. The coastal typology classification near Saunton Sands (Devon, UK), shown at its 100 m alongshore resolution for each of the four tasks: (A) *sediment type*, (B) *coastal type*, (C) *is built environment*, and (D) *has defense*. Insets in each panel show supporting photographs sourced from public imagery. The example illustrates how the model distinguishes subtle variations across the four classification tasks, including dunes along Saunton Sands (Inset A), sediment plains and coastal defenses near Westward Ho! (Inset B), built environment at Instow (Inset C), and the absence of defenses around Croyde despite nearby development (Inset D). The basemap is from Esri World Imagery. This example illustrates the resolution and interpretability of the coastal classification at local scale.

https://doi.org/10.5194/essd-2025-388
Preprint. Discussion started: 24 July 2025

Open Access Earth System Science Data Discussions

(22%) and sandy shores (24%), reflecting their geomorphic variability. Inlets are most often matched with sandy shorelines (89%), consistent with their dynamic and nature that is rich in sandy sediments. Engineered structures are strongly linked to sediment-free shorelines (74%), suggesting that hard-structure interventions tend to disrupt natural sediment presence or occur where it is entirely absent. Likewise, coastal defenses are overwhelmingly situated near built environments: 83% of defended coastlines also contain built environment (Fig. 7).

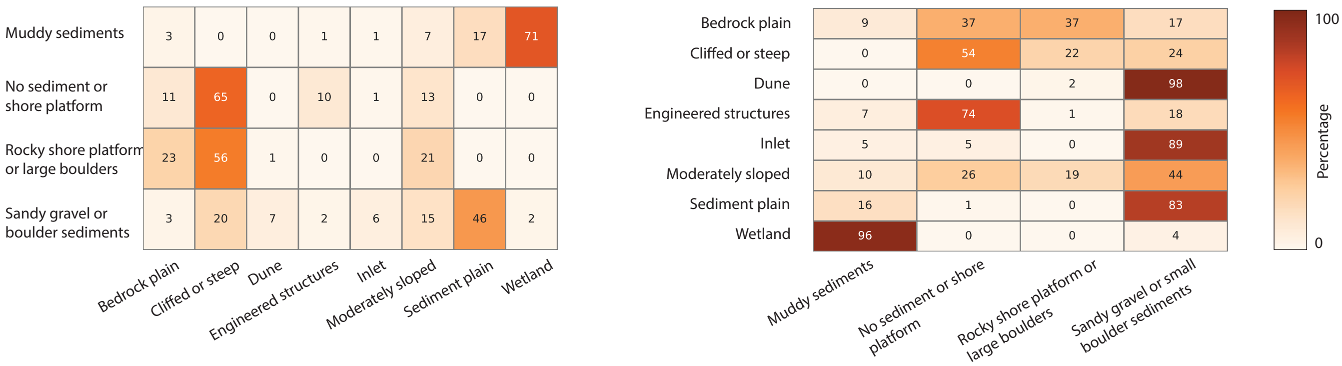

Figure 6. Normalized co-occurrence matrices between *shore_type* and *coastal_type*. Each row represents a single class from the source task (either shore or coastal type), and each column indicates the percentage of samples co-labeled with a given class from the other task. Values are normalized such that each row sums to 100%, enabling a direct interpretation of conditional relationships between classification tasks. This visualization highlights systematic co-occurrence patterns and supports interpretation of typological compatibility.

3.5 Data Records

The coastal typology dataset (Calkoen et al., 2025b) released in this study contains model predictions for four coastal typology tasks: *sediment type*, *coastal type*, *has defense*, and *is built environment*. Each record corresponds to a unique transect in the GCTS and includes both the predicted class label and a corresponding model confidence score for each task.

For multi-class tasks (*sediment type*, *coastal type*), probabilities are computed using the softmax function and reported per class. For binary tasks, probabilities are derived from the sigmoid function and indicate the likelihood of a positive prediction, using a threshold of 0.5 for classification. Probabilities are stored in columns prefixed with *prob_**, followed by the class name (e.g., *prob_muddy_sediments*) or task name (e.g., *prob_has_defense*). To enhance downstream coastal analytics, each record includes some key metadata (copied over from GCTS), including the unique transect ID, geographic coordinates, bounding box, administrative region, and tile identifier.

Table 5 summarizes all structured fields, including data types, value ranges, and source attribution. The dataset is stored as partitioned Parquet files, organized by coastal grid tile, and available under a CC-BY-4.0 license. It spans the global coastline between $-70°$ and $70°$ latitude while including Iceland, uses EPSG:4326 as its spatial reference system, and reflects Sentinel-2 satellite imagery of 2023. Data can be accessed via a the CoCliCo STAC catalog, with instructions and an example notebook

https://doi.org/10.5194/essd-2025-388
Preprint. Discussion started: 24 July 2025

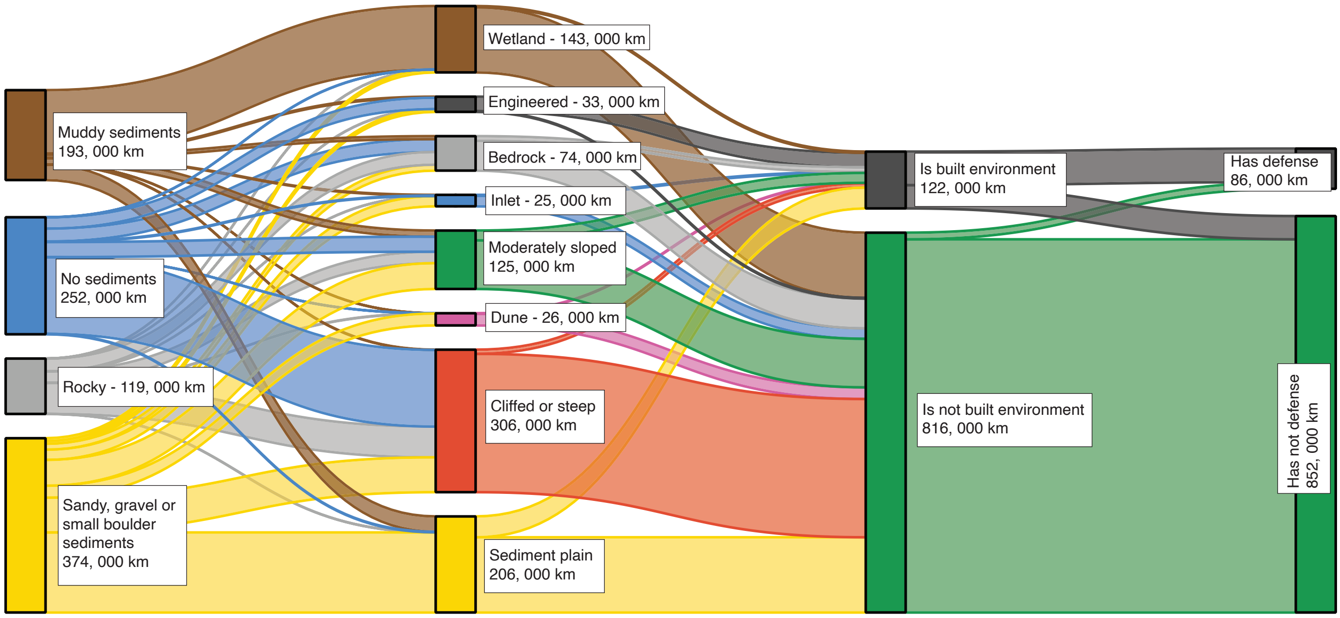

Figure 7. Sankey diagram showing the co-distribution of predicted classes across four typology dimensions: *sediment type*, *coastal type*, *is built environment* and *has defense*. Each vertical layer represents one classification task, with all categories in each task summing to the global coastline length in kilometers. The thickness of each flow segment is proportional to the coastline length shared between two connected class labels. This visualization highlights common transitions and conditional relationships between coastal typologies, such the relatively large share of sandy, gravel or small boulder sediments that is backed by cliffed or steep coasts.

available in the `CoastPy` GitHub repository (Calkoen et al., 2025c). The data is also archived at Zenodo https://doi.org/10.5281/zenodo.15599096.

4 Discussion

This study makes two distinct contributions: first, it provides better and previously unknown global estimates of the distribution and composition of coastal systems; second, it represents a methodological advance by introducing deep learning into coastal science for broad-scale coastal analysis of satellite data. The following subsections first discuss the results of our coastal classification by comparing the estimates to existing coastal typologies, then state the inherent assumptions made in the methodology, evaluate the model's performance, and finally highlight methodological innovations.

4.1 The global distribution and composition of coastal systems

Quantifying the global distribution and composition of coastal systems has a long history in coastal science, with estimates varying widely depending on methodology and data availability. An early expert-based inventory (Bird, 1985) estimated that approximately 20% of the world's coastlines are sandy. In contrast, more recent large-scale satellite-based approaches have

https://doi.org/10.5194/essd-2025-388
Preprint. Discussion started: 24 July 2025

Open Access Earth System Science Data Discussions

Table 5. Structured output fields in the geospatial classification dataset. Each field is defined by its name, description, data type, value range or format, and source.

Field Name	Description	Data Type	Range / Format	Source
transect_id	Unique GCTS ID; foundational reference	string	–	GCTS
geometry	Centroid point (longitude, latitude)	geometry	EPSG:4326	GCTS
bbox	Bounding box coordinates	array[float]	[minx, miny, maxx, maxy]	GCTS
quadkey	Microsoft tile identifier	string	QuadKey	GCTS
utm_epsg	UTM projection code	int32	e.g., 32633	GCTS
continent	Continent name	string	–	GCTS
country	Country code (ISO2)	string	ISO2	GCTS
common_country_name	Country name (long form)	string	–	GCTS
common_region_name	Administrative region name	string	–	GCTS
shore_type	Predicted sediment type class	categorical	4 classes	Model
coastal_type	Predicted coastal type class	categorical	8 classes	Model
is_built_environment	Predicted built environment presence	boolean	True / False	Model
has_defense	Predicted coastal defense presence	boolean	True / False	Model
prob_* (N=14)	Class probabilities (per task)	float32	[0–1]	Model

reported higher figures; Luijendijk et al. (2018) find that 31% of global ice-free coastlines are sandy. In our study, we estimate that 40% of the world's coastlines are sandy, gravel or shingle, amounting to 375,000 km between 70°N and 70°S. This higher figure primarily reflects improvements in spatial sampling. Unlike earlier studies based on Web Mercator-derived transects, we use the Global Coastal Transect System (GCTS), which distributes transects evenly (every 100 m) in latitude and thereby corrects zonal biases (Calkoen et al., 2025c). Attributing the difference to the transect system used is supported by a continental comparison: In Africa, where zonal distortion is minimal, our estimate of 65% sandy coastlines closely matches the 67% reported by Luijendijk et al. (2018). This agreement occurs despite differences in classification criteria, including a minimum beach width of 20 m and the exclusion of small boulder beaches in the earlier study, both of which are included in the present classification.

For muddy coasts, Hulskamp et al. (2023) reported a global figure of 14%, noting their prevalence in equatorial and deltaic regions. Our estimate is substantially higher at 21% (193,000 km), a difference that can again be attributed to usage of a latitudinally-consistent transect system (GCTS), which better captures the footprint of equatorial muddy coastlines such as those in Southeast Asia, West Africa, and the Amazon delta. An additional factor is the classification schema: whereas Hulskamp et al. (2023) include a separate class for "vegetated" coasts, our model does not distinguish vegetated systems explicitly because we focus on the geomorphology. Many such coasts—especially in estuarine deltas—are both vegetated and muddy, suggesting overlap between their vegetated class and our muddy class.

These comparisons with Luijendijk et al. (2018) and Hulskamp et al. (2023) underline the foundational role of GCTS in global coastal analytics. By using a geographically uniform transect system, we reduce latitudinal sampling bias and accurately

https://doi.org/10.5194/essd-2025-388
Preprint. Discussion started: 24 July 2025

capture equatorial coastlines. Also, GCTS is derived from a more recent OpenStreetMap coastline, hence, has broader and better spatial coverage.

Despite their geomorphological significance and hazard mitigation, dune coasts are relatively rare on a global scale. Our analysis indicates that they comprise 3% of the world's coastline (26,000 km), a relatively short length, especially when contrasted to sandy shorelines more broadly, that account for 40% (375,000 km). This disparity probably reflects the specific formation requirements for dune systems (Moore et al., 2025)—including large sand supply, persistent onshore winds, and sufficient space for inland accumulation—which are not consistently met across most coastal regions. Human impacts may further contribute to their scarcity, as many dune systems have been flattened or modified for coastal development (Lansu et al., 2024). Given the relatively modest classification performance for dune coasts (F1 = 0.65), these findings should be interpreted with caution. Some dune systems may be misclassified into adjacent categories; most notably *moderately sloped* coasts, as shown in a local example (Fig. 5, panel B), where dunes are labeled as moderately slopedis.

Young and Carilli (2019) showed that cliffed coastlines are widespread globally, with 93% of the world's coastal regions containing some cliffed segments. However, their estimate was based on regional presence across 213 coastal units, rather than on proportional shoreline length. In this study, we provide the first globally consistent, length-based estimate of cliff coasts: approximately 33% of the global coastline, or 305,000 km between 70°N and 70°S, is cliffed or steep.

Our classification also enables cross-shore compositional analysis. For example, we find that approximately 20% of sandy coastlines are backed by cliffs or steep slopes (74,000 km). These cliff-backed beaches are of particular concern under rising sea levels (Vitousek et al., 2017), as they typically combine limited sediment supply with minimal room for inland migration, making them among the systems most vulnerable to beach loss and morphological collapse in the coming centuries.

Recent global assessments have quantified "coastal squeeze" (Lansu et al., 2024) and "coastal hardening" (Nawarat et al., 2024), providing insight into the extent of human modification along sandy shorelines. Lansu et al. (2024) report that 33% of sandy coasts have less than 100 m of infrastructure-free space inland, while Nawarat et al. (2024) estimate that 33% are "hardened." In our analysis, we apply more conservative guidelines based on visual interpretation of satellite imagery, supported by self-supervised machine learning. Using this approach, we estimate that 16.5% of sandy, gravel or small boulder shorelines are embedded within built environments, such as settlements or ports and 9.3% have visible coastal defenses. The dataset shows that 11% of the continental European coastline features human-made coastal defenses, substantially higher than the 5% previously reported by EUROSION (Salman et al., 2004). This discrepancy may reflect expanded detection through our automated methods, and/or an actual increase in coastal defenses since that study, and/or potential overclassification due to false positives in the model. Only 3% of sandy shores are classified as engineered coasts—locations where the natural geomorphology is visibly inactive due to heavy human intervention (e.g., port development). Notably, this engineered category is more prevalent in Asia, consistent with widespread recent coastal development in the region. Overall, these findings align with earlier work showing that coastal populations are concentrated in specific regions (McGranahan et al., 2007; Kulp and Strauss, 2019)—particularly in South, Southeast, and East Asia, as well as mid- and low-latitude deltas and cities—while large lengths of coast have little or no direct population pressure (Small and Nicholls, 2003; Lincke and Hinkel, 2018).

https://doi.org/10.5194/essd-2025-388
Preprint. Discussion started: 24 July 2025

4.2 Methodological assumptions

While this study is not constrained by data availability—satellite Earth observations are global and relatively consistent—our methodology relies on several assumptions. First, the classification presented here is not a fixed taxonomy but a functional typology, intended to support consistent, large-scale analyses of coastal change and erosion risk. Like any typology, it simplifies a naturally continuous landscape: transitional forms may fall between classes, and certain lithological nuances (e.g., distinctions between hard and soft rock) remain beyond the resolution of satellite-based observation.

Second, the classifier uses a supervised learning approach that necessarily reflects the characteristics of its training dataset. In this study, the majority of training samples (approximately 95%) were provided by the lead author. As such, the resulting typology inevitably reflects the judgments and interpretation of that individual. This is a common limitation of broad-scale remote sensing studies that rely on learning-based methods (including tree-based or deep learning approaches), where expert-driven labeling is fundamental to model training. Uncertainty also varies across the classified attributes: sediment type builds on well-established categories and is comparatively robust, whereas coastal type, built environment, and coastal defense are subject to greater interpretative ambiguity due to less standardized definitions.

4.3 Model performance

The model demonstrates strong and consistent performance across all four typology tasks, with accuracy scores varying according to task complexity, class prevalence and geomorphological ambiguity in the coastal typology.

Binary tasks—*is built environment* and *has defense*—achieved the highest macro-F1 scores of 0.83 and 0.77, respectively, with low variability across runs (standard deviations ≤ 0.04). Multi-class tasks were more challenging due to the finer morphological distinctions and greater number of classes: *sediment type* reached a macro-F1 of 0.76, while *coastal type* scored 0.68.

At the class level, performance also varied. Classes with distinct spectral or morphological features, such as *muddy sediments* (F1 = 0.86), *sandy, gravel or small boulder sediments* (F1 = 0.84) and *wetlands* (F1 = 0.77), were classified with high accuracy, also suggesting that clear visual cues can offset limited training data (e.g., *muddy sediments* and *wetlands*). Conversely, classes with more ambiguous or transitional characteristics—such as *moderately sloped* (F1 = 0.55)—showed lower performance, likely due to their overlap with adjacent classes like *cliffed*, *dune*, and *sediment plain*. Similarly, *dune* coasts yielded a modest F1-score (0.65), reflecting spectral similarity with nearby categories, particularly *sediment plains*, which explicitly include beach ridge systems that can resemble dunes in satellite imagery. For *inlet* (F1 = 0.61), performance varied more across runs, possibly indicating inconsistencies in the training data set for this class.

Despite a relatively small training set (N = 1800), the model exhibited consistent behavior across 10 independent training runs, with low variance in most metrics. While there is a broad correlation between class frequency and performance, exceptions suggest that feature distinctiveness and annotation clarity are also influential. To support future improvements, the annotation tool used for labeling is made publicly available, and we actively invite new contributions from the coastal science community to extend coverage in underrepresented areas or class types.

https://doi.org/10.5194/essd-2025-388
Preprint. Discussion started: 24 July 2025

Open Access Earth System Science Data Discussions

Model confidence scores during inference (Fig. D2) indicate high model certainty outside Europe, but this should be interpreted cautiously, as confidence does not necessarily imply true generalization quality. However, confidence levels are broadly consistent across regions and vary more strongly by class, implying that uncertainty arises from typological ambiguity rather than geographic region, supporting the model's global applicability.

4.4 Methodological advances

A notable strength of our approach is that it relies exclusively on satellite imagery and elevation data, without incorporating ancillary geospatial variables such as climatic conditions (e.g., wave regime, temperature) or other geospatial data products (e.g., CORINE Land Cover). This design choice minimizes the risk of data leakage from environmental drivers into the classification process, thereby preserving the integrity of downstream analyses. As a result, correlations between coastal typology and external forcing factors—such as climate or socioeconomic variables—can be investigated without introducing circularity or confounding effects.

Another strength of our method is the region-of-interest (400 m x 2000 m) encoding within each image chip (2.8 km x 2.8 km). Each prediction is made for a 400 m alongshore by 2 km cross-shore region (region of interest, that is spatially encoded), while the model sees the broader a 2.8 km $\times$ 2.8 km area, providing additional context. In addition, the landward and seaward direction of the transect is encoded, so that model knows which coast to consider when classifying areas with narrow bays. Overall this setup enables the model to integrate local detail with the surrounding area, as seen in the Saunton Sands example (Section 3.3), where it accurately resolves transitions between dunes, sediment plains, rocky shores, urbanized segments, and pocket beaches like Croyde.

Recent efforts by Hanson et al. (2025) and Nyberg et al. (2025) continue the tradition of rule-based coastal classification, building on frameworks such as EUROSION and DIVA. These approaches are well-established and integrate geomorphological expertise with ancillary data to characterize the coast at broad scale. In contrast, our deep learning-based method is fully automated, relying solely on satellite imagery and elevation data, and can be efficiently updated and/or expanded. While promising for global-scale analysis, it represents an emerging approach; the typology definitions may require further refinement, and the training dataset would benefit from contributions by a broader expert community.

Many typological classes in this study span multiple pixels and are characterized by contextual spatial patterns (e.g., dunes, wetlands, and defense structures, among others). Deep learning models naturally accommodate such patterns by learning spatial dependencies, in contrast to traditional pixel-wise or feature-based classifiers (e.g., Random Forest) that often require manually engineered features or hybrid models. Adopting deep learning, reduces the need for complex rule-based postprocessing and enables end-to-end learning from raw data. Overall, the accuracy scores for sandy and muddy sediment types are comparable to those of Hulskamp et al. (2023), who report F1-scores of 75% (sandy) and 87% (muddy) using a hybrid tree-based approach incorporating, that includes ancillary geospatial datasets. So, while using a smaller training dataset, without providing ancillary geospatial datasets as inputs, we report better accuracy scores for the deep learning model than has been previously reported for tree-based classifiers.

https://doi.org/10.5194/essd-2025-388
Preprint. Discussion started: 24 July 2025

Open Access Earth System Science Data Discussions

In the introduction, we highlighted two major developments that have transformed coastal science: the opening-up of Earth observation data and the emergence of user-friendly cloud platforms. This study represents a third step in this evolution, demonstrating how integrating deep learning (or broader AI) with these capabilities provides a natural and powerful solution for capturing the complexity of coastal environments globally. Uniting these three advancements (open satellite data, cloud technology, and artificial intelligence) arguably shows the full potential of modern, data-driven coastal analytics. Crucially, individually, each component has limitations: without open data, research will be unequal, disadvantaging those with less means and lack reproducibility; without cloud technology, scaling from experimental case studies to consistent global applications remains challenging or simply not possible; and without AI, analysis is constrained to traditional machine learning methods unable to handle the complexity of real-world coastal systems. Only by combining all three can we can advance high-resolution, data-driven coastal science globally.

5 Conclusions

The combination of open satellite archives and cloud technology has fundamentally transformed how we study the Earth's coastlines. This study marks a third step in that evolution, demonstrating how integrating deep learning with these capabilities provides a more natural and especially more powerful solution for studying complex coastal systems globally.

The multi-task deep learning model shows strong performance across all four classifications tasks, with performance depending on task complexity, class prevalence and geomorphological ambiguity in the coastal typology. Binary classifications—identifying built environments (F1: 0.83) and coastal defenses (F1: 0.77)—achieve the highest accuracy due to their task simplicity. Performance remains strong for sediment type classification, particularly for clearly defined categories such as sandy (F1: 0.84) and muddy sediments (F1: 0.86). However, classification accuracy decreases for the more complex coastal type classification, especially for the transitional coastal types such as moderately sloped (F1: 0.55) and inlets (F1: 0.61) that have high morphological ambiguity, but are for some classes also negatively affected by the limited amount of training data (e.g., dune coasts) as well as labeling consistency within the training samples (inlets). A notable strength of the method is its reliance solely on satellite data, ensuring unbiased downstream analyses of relationships between coastal types and external environmental conditions.

The dataset offers comprehensive and accurate global estimates of coastal sediment composition, indicating that approximately 40% of global coastlines consist of sandy, gravel, or shingle sediments, 21% are muddy, 13% rocky, and 27% are sediment-free. This shows that over 60% of the world's coastlines are composed of soft sediments, which are easily erodible. Geomorphologically, about 33% of coasts are cliffed, 22% sediment plains, 15% wetlands, and only 3% are dune systems (adding up to 26,000 km), the rarity of which likely reflects specific formation requirements and widespread human alteration.

The cross-shore composition of coastal systems further emphasizes coastal vulnerability: 20% of sandy coastlines are cliff-backed, posing significant risks under accelerating sea-level rise due to limited space for inland retreat. Additionally, 16.5% of sandy coasts are embedded within built environments, which are regions that are particularly susceptible to "coastal squeeze" and human-induced modification. A final notable finding is that 9.3% of the world's coastline features visible coastal defenses, with 59% of built-up coasts also containing coastal defenses and, conversely, 83% of defended coasts situated along built-up areas.

As an automated, data-driven method, the typology can be efficiently refined over time—through improved class definitions, targeted corrections, and expanded training data to reduce expert bias and geographic imbalance. Overall, the dataset may support numerous applications, including coastal change monitoring, erosion risk assessments, and broad-scale vulnerability mapping, thereby providing a critical foundation for coastal adaptation planning in response to accelerating climate change.

Code and data availability. All data, code, and models used in this study are openly available. The coastal typology dataset is published as partitioned, cloud-optimized Parquet files and can be accessed through the CoCliCo STAC catalog. A static archive is also available via Zenodo: https://doi.org/10.5281/zenodo.15599096 (Calkoen et al., 2025b). The deep learning model code used to produce the typology is available through the open-source `CoastPy` package at https://github.com/COCLICO/coastpy (Calkoen et al., 2025c).

Sample availability. The training samples used to develop the coastal typology model are released as the CoastBench dataset (Calkoen et al., 2025a), available under a CC-BY-4.0 license. The dataset includes annotated labels for sediment type, coastal type, and the presence of built environment and coastal defenses. It is available at https://doi.org/10.5281/zenodo.15800285. The dataset is accessible through a STAC collection and can be expanded via a custom web application. The source code for the application is available at https://github.com/florisCalkoen/coastapp.

https://doi.org/10.5194/essd-2025-388
Preprint. Discussion started: 24 July 2025

Appendix A: Global coastal typology

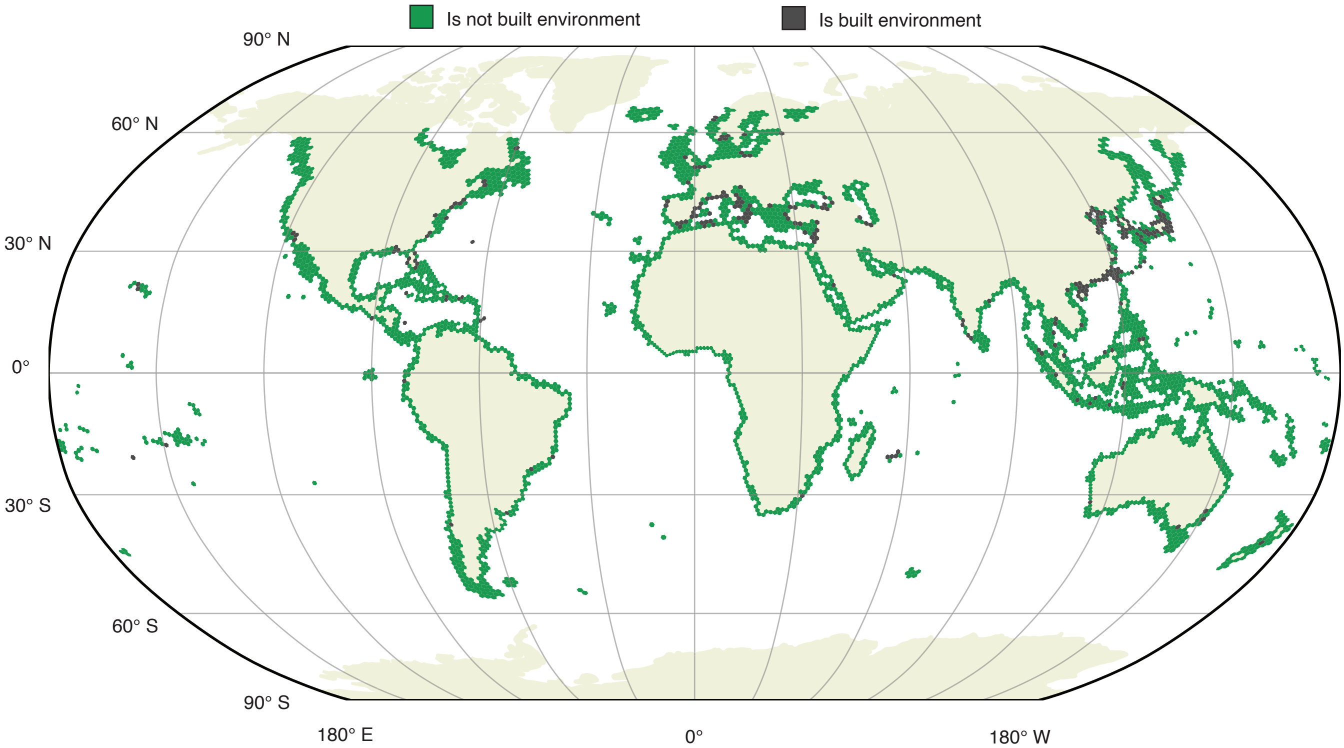

Figure A1. Global map of predicted *is built environment*, aggregated on a level-3 H3 grid for visualization purposes using the most frequent class (mode) per cell. This coarser view summarizes almost 10 million classified coastal transects, highlighting regional patterns. Basemap: Natural Earth.

https://doi.org/10.5194/essd-2025-388
Preprint. Discussion started: 24 July 2025

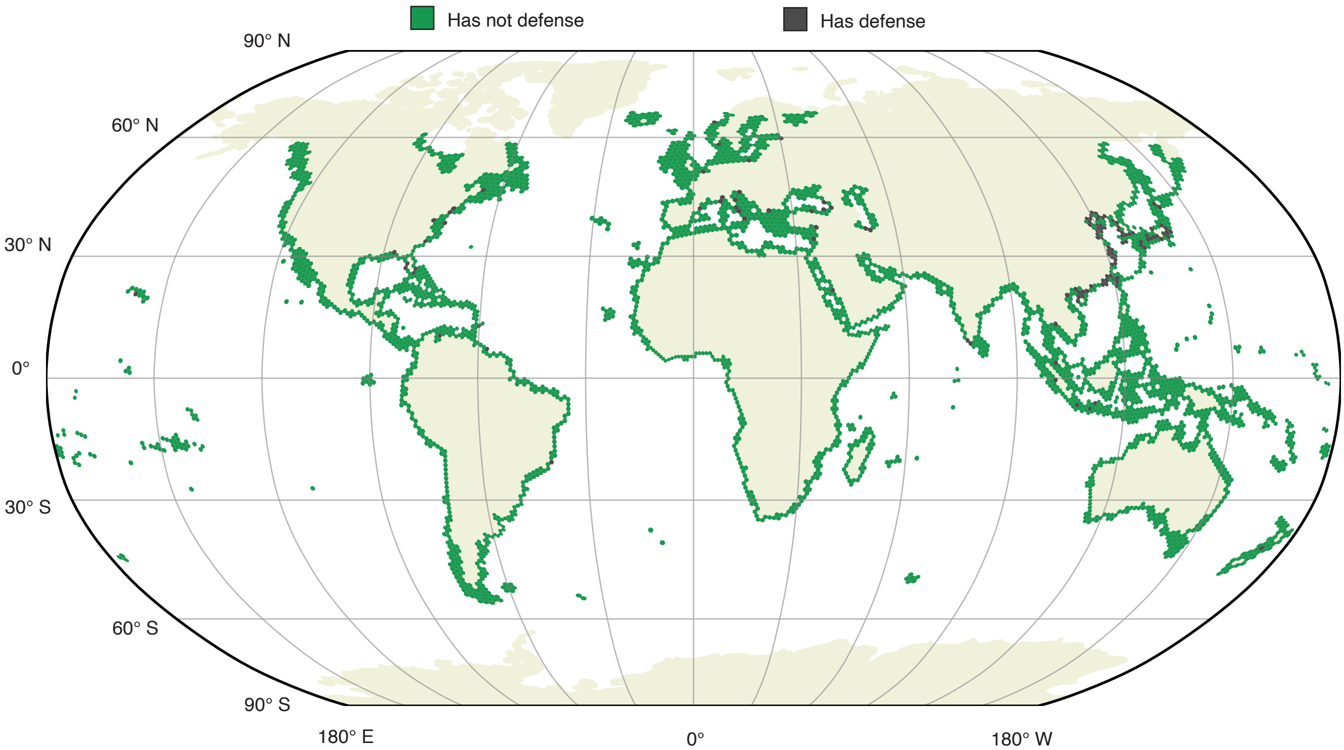

Figure A2. Global map of predicted *has defense*, aggregated on a level-3 H3 grid for visualization purposes using the most frequent class (mode) per cell. This coarser view summarizes almost 10 million classified coastal transects, highlighting regional patterns. Basemap: Natural Earth.

https://doi.org/10.5194/essd-2025-388
Preprint. Discussion started: 24 July 2025

Appendix B: European Coastal typology

Figure B1. Map of continental Europe with predicted *sediment type*, aggregated on a level-5 H3 hexagonal grid for visualization purposes using majority class (mode) per cell. This continental view summarizes around 1.2 million classified coastal transects, highlighting regional patterns. Basemap: Natural Earth.

https://doi.org/10.5194/essd-2025-388
Preprint. Discussion started: 24 July 2025

Open Access Earth System Science Data Discussions

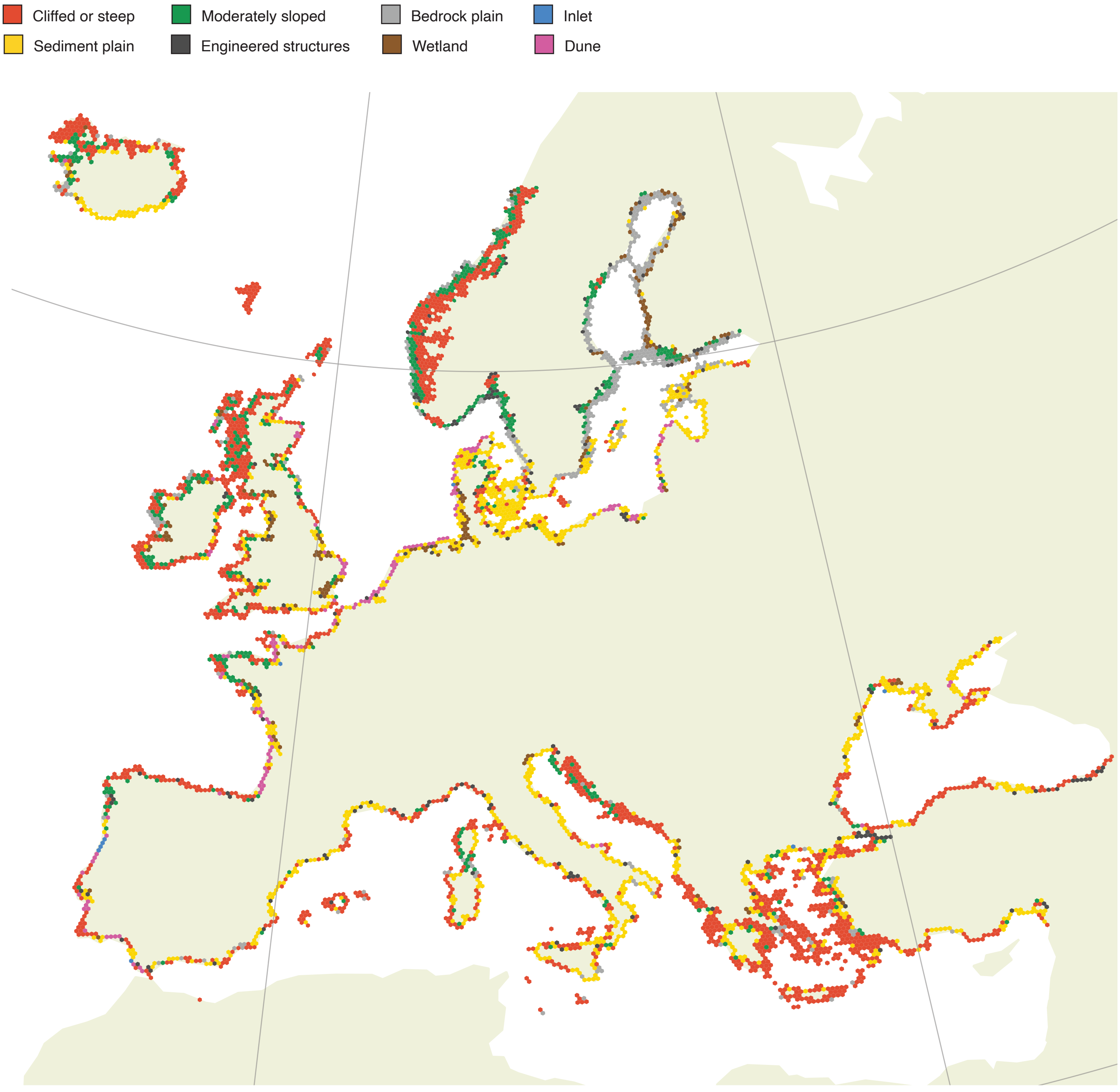

Figure B2. Map of continental Europe with predicted *coastal type*, aggregated on a level-5 H3 hexagonal grid using majority class (mode) per cell. This continental view summarizes around 1.2 million classified coastal transects, highlighting regional patterns. Basemap: Natural Earth.

https://doi.org/10.5194/essd-2025-388
Preprint. Discussion started: 24 July 2025

Appendix C: Coastal typology per country

https://doi.org/10.5194/essd-2025-388
Preprint. Discussion started: 24 July 2025

Open Access
Earth System Science Data
Discussions

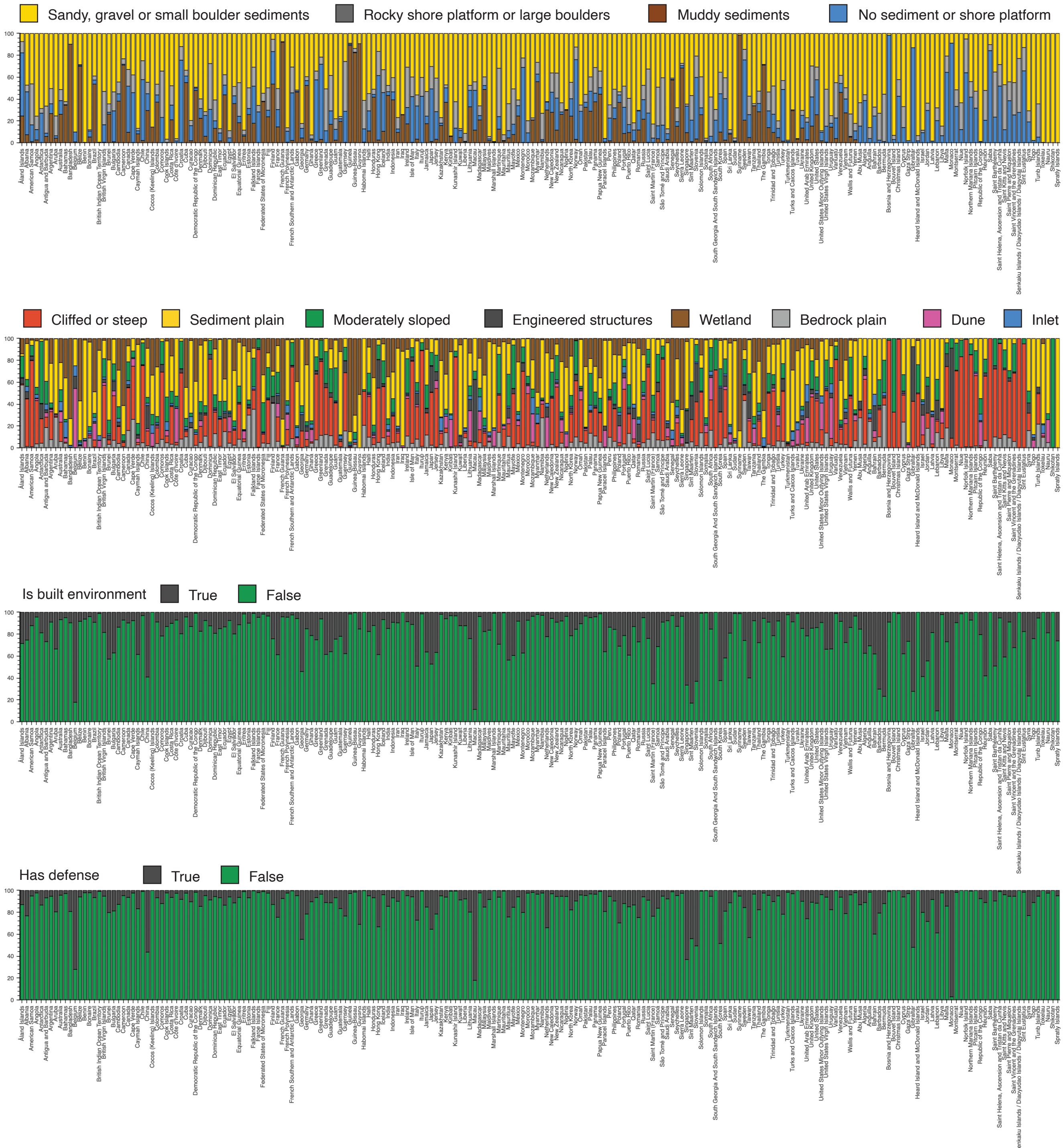

Figure C1. Normalized class distributions per country for each of the four classification tasks: *sediment type*, *coastal type*, *is_built_environment*, and *has_defense*. For each task, stacked bars represent the percentage of transects assigned to each class within a given country. This allows for comparative analysis of coastal typology across countries.

https://doi.org/10.5194/essd-2025-388
Preprint. Discussion started: 24 July 2025

Appendix D: Classification performance

480 ### D1 Global distribution of training samples

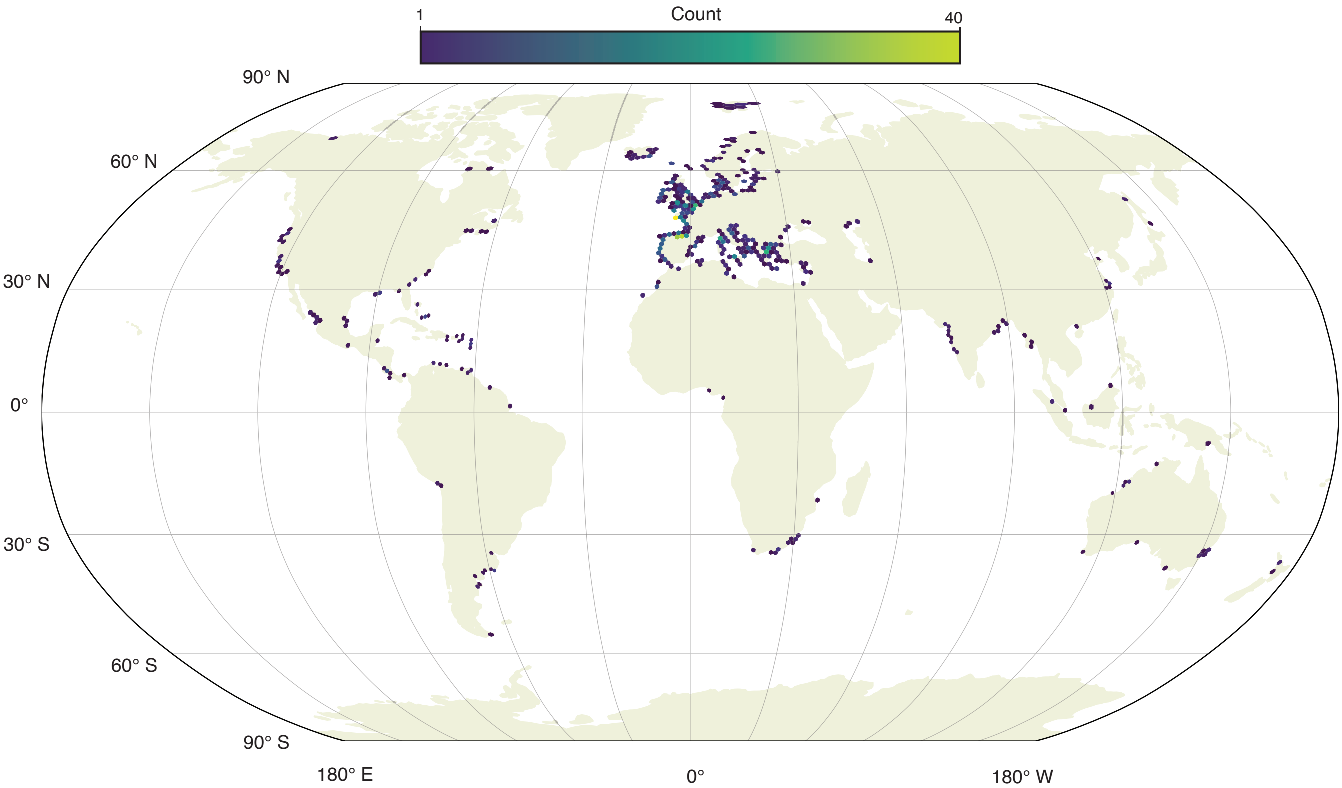

Figure D1. Global distribution of training samples per H3 cell (zoom level 3). Basemap: Natural Earth.

https://doi.org/10.5194/essd-2025-388
Preprint. Discussion started: 24 July 2025

D2 Classification Confidence and Uncertainty

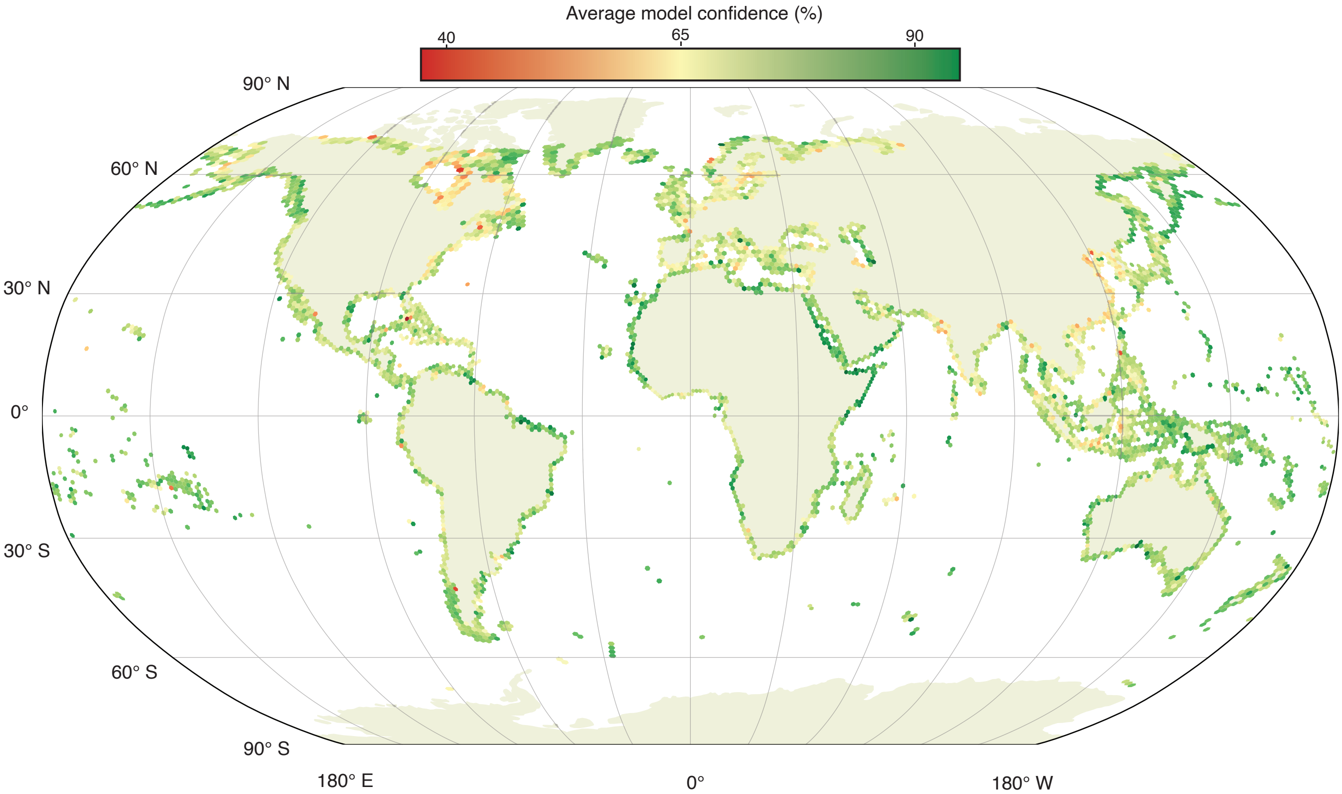

Figure D2. Model confidence per H3 cell (zoom level 3) averaged across the four typology tasks. Confidence is computed for each transect as follows: for multi-class tasks (*shore_type*, *coastal_type*), it is defined as the maximum predicted class probability; for binary tasks (*has_defense*, *is_built_environment*), it is the distance from the classification threshold (0.5), scaled between 0 and 100. This visualization highlights regions where model predictions are more certain (green) or more ambiguous (red), providing spatial insight into model reliability. Basemap: Natural Earth.

https://doi.org/10.5194/essd-2025-388
Preprint. Discussion started: 24 July 2025

Author contributions. Conceptualization: FC, AL, RN, SH. Methodology and formal analysis: FC. Software and infrastructure: FC, FB. Machine learning model design and optimization: FC, AMR, HdH. Supervision and guidance: AL and RN. Writing – original draft: FC. Writing – review and editing: all authors.

Competing interests. The authors declare that they have no competing interests.

Disclaimer. This study represents the views of the authors and does not necessarily reflect those of their affiliated institutions.

Acknowledgements. We thank all contributors who provided classification labels to the CoastBench training dataset; their efforts made the development of this dataset possible. We are also grateful to Roshanka Ranasinghe and Stefan Aarninkhof for the numerous discussions we had on the topic, and in Ranasinghe's case, for his feedback on the draft manuscript. We also acknowledge the use of AI-based tools to support code development and improve grammar during manuscript preparation.

References

Barnard, P. L., Befus, K. M., Danielson, J. J., Engelstad, A. C., Erikson, L. H., Foxgrover, A. C., Hayden, M. K., Hoover, D. J., Leijnse, T. W. B., Massey, C., McCall, R., Nadal-Caraballo, N. C., Nederhoff, K., O'Neill, A. C., Parker, K. A., Shirzaei, M., Ohenhen, L. O., Swarzenski, P. W., Thomas, J. A., van Ormondt, M., Vitousek, S., Vos, K., Wood, N. J., Jones, J. M., and Jones, J. L.: Projections of Multiple Climate-Related Coastal Hazards for the US Southeast Atlantic, Nature Climate Change, 15, 101–109, https://doi.org/10.1038/s41558-024-02180-2, 2025.

Biewald, L.: Experiment Tracking with Weights and Biases, 2020.

Bird, E. C. F.: Coastline Changes. A Global Review, 1985.

Brown, C. F., Brumby, S. P., Guzder-Williams, B., Birch, T., Hyde, S. B., Mazzariello, J., Czerwinski, W., Pasquarella, V. J., Haertel, R., Ilyushchenko, S., Schwehr, K., Weisse, M., Stolle, F., Hanson, C., Guinan, O., Moore, R., and Tait, A. M.: Dynamic World, Near Real-Time Global 10 m Land Use Land Cover Mapping, Scientific Data, 9, 251, https://doi.org/10.1038/s41597-022-01307-4, 2022.

Buscombe, D. D., Wernette, P., Fitzpatrick, S., Favela, J., Goldstein, E. B., and Enwright, N.: A 1.2 Billion Pixel Human-Labeled Dataset for Data-Driven Classification of Coastal Environments, 2022.

Calkoen, F. R., Luijendijk, A. P., Hanson, S., Nicholls, R., Moreno Rodenas, A., De Heer, H., and Baart, F.: CoastBench: A Global Training Dataset for Coastal Classification Using Satellite Imagery and Elevation Data, https://doi.org/10.5281/zenodo.15800285, 2025a.

Calkoen, F. R., Luijendijk, A. P., Hanson, S., Nicholls, R., Moreno Rodenas, A., De Heer, H., and Baart, F.: Mapping the World's Coast: A Global 100 m Coastal Typology Derived from Satellite Data Using Deep Learning, https://doi.org/10.5281/zenodo.15607678, 2025b.

Calkoen, F. R., Luijendijk, A. P., Vos, K., Kras, E., and Baart, F.: Enabling Coastal Analytics at Planetary Scale, Environmental Modelling & Software, 183, 106 257, https://doi.org/10.1016/j.envsoft.2024.106257, 2025c.

Çelik, O. İ.: Leveraging Deep Learning for Coastal Monitoring: A VGG16-based Approach to Spectral and Textural Classification of Coastal Areas with Sentinel-2A Data, Applied Ocean Research, 2024.

Christen, P., Hand, D. J., and Kirielle, N.: A Review of the F-Measure: Its History, Properties, Criticism, and Alternatives, ACM Comput. Surv., 56, 73:1–73:24, https://doi.org/10.1145/3606367, 2023.

Cooper, J. A. G. and McLaughlin, S.: Contemporary Multidisciplinary Approaches to Coastal Classification and Environmental Risk Analysis, Journal of Coastal Research, 14, 512–524, 1998.

Dang, K. B., Dang, V. B., Bui, Q. T., Nguyen, V. V., Pham, T. P. N., and Ngo, V. L.: A Convolutional Neural Network for Coastal Classification Based on ALOS and NOAA Satellite Data, IEEE Access, 8, 11 824–11 839, https://doi.org/10.1109/ACCESS.2020.2965231, 2020.

European Environment Agency.: European Climate Risk Assessment., Publications Office, LU, 2024.

European Space Agency (ESA): Copernicus DEM - Global and European Digital Elevation Model, https://doi.org/10.5270/ESA-c5d3d65, 2019.

Fairbridge, R. W.: Classification of Coasts, Journal of Coastal Research, 20, 155–165, https://doi.org/10.2112/1551-5036(2004)20[155:COC]2.0.CO;2, 2004.

Finkl, C. W.: Coastal Classification: Systematic Approaches to Consider in the Development of a Comprehensive Scheme, Journal of Coastal Research, 20, 166–213, 2004.

Finkl, C. W. and Makowski, C.: Coastal Belt Linked Classification (CBLC): A System for Characterizing the Interface between Land and Sea Based on Large Marine Ecosystems, Coastal Ecological Sequences, and Terrestrial Ecoregions, Journal of Coastal Research, 36, 677–693, https://doi.org/10.2112/JCOASTRES-D-20A-00001.1, 2020.

French, J., Burningham, H., Thornhill, G., Whitehouse, R., and Nicholls, R. J.: Conceptualising and Mapping Coupled Estuary, Coast and Inner Shelf Sediment Systems, Geomorphology, 256, 17–35, https://doi.org/10.1016/j.geomorph.2015.10.006, 2016.

Gorelick, N., Hancher, M., Dixon, M., Ilyushchenko, S., Thau, D., and Moore, R.: Google Earth Engine: Planetary-scale Geospatial Analysis for Everyone, Remote Sensing of Environment, 202, 18–27, https://doi.org/10.1016/j.rse.2017.06.031, 2017.

Hamman, J., Rocklin, M., and Abernathy, R.: Pangeo: A Big-data Ecosystem for Scalable Earth System Science, p. 12146, 2018.

Hanson, S., Nicholls, R. J., Balson, P., Brown, I., French, J. R., Spencer, T., and Sutherland, W. J.: Capturing Coastal Geomorphological Change within Regional Integrated Assessment: An Outcome-Driven Fuzzy Logic Approach, Journal of Coastal Research, 265, 831–842, https://doi.org/10.2112/JCOASTRES-D-09-00078.1, 2010.

Hanson, S. E., Nicholls, R. J., Calkoen, F. R., Le Cozannet, G., and Luijendijk, A. P.: A Geospatial Database of Coastal Characteristics for Erosion Assessment of Europe's Coastal Floodplains, https://doi.org/10.5194/egusphere-2025-2371, 2025.

Hayes, M. O.: Relationship between Coastal Climate and Bottom Sediment Type on the Inner Continental Shelf, Marine Geology, 5, 111–132, https://doi.org/10.1016/0025-3227(67)90074-6, 1967.

He, K., Zhang, X., Ren, S., and Sun, J.: Deep Residual Learning for Image Recognition, in: 2016 IEEE Conference on Computer Vision and Pattern Recognition (CVPR), pp. 770–778, IEEE, Las Vegas, NV, USA, ISBN 978-1-4673-8851-1, https://doi.org/10.1109/CVPR.2016.90, 2016.

Hinkel, J., Nicholls, R. J., Tol, R. S. J., Wang, Z. B., Hamilton, J. M., Boot, G., Vafeidis, A. T., McFadden, L., Ganopolski, A., and Klein, R. J. T.: A Global Analysis of Erosion of Sandy Beaches and Sea-Level Rise: An Application of DIVA, Global and Planetary Change, 111, 150–158, https://doi.org/10.1016/j.gloplacha.2013.09.002, 2013.

Hulskamp, R., Luijendijk, A., van Maren, B., Moreno-Rodenas, A., Calkoen, F., Kras, E., Lhermitte, S., and Aarninkhof, S.: Global Distribution and Dynamics of Muddy Coasts, Nature Communications, 14, 8259, https://doi.org/10.1038/s41467-023-43819-6, 2023.

Killough, B.: Overview of the Open Data Cube Initiative, in: IGARSS 2018 - 2018 IEEE International Geoscience and Remote Sensing Symposium, pp. 8629–8632, IEEE, Valencia, ISBN 978-1-5386-7150-4, https://doi.org/10.1109/IGARSS.2018.8517694, 2018.

Kulp, S. A. and Strauss, B. H.: New Elevation Data Triple Estimates of Global Vulnerability to Sea-Level Rise and Coastal Flooding, Nat Commun, 10, 4844, https://doi.org/10.1038/s41467-019-12808-z, 2019.

Lansu, E. M., Reijers, V. C., Höfer, S., Luijendijk, A., Rietkerk, M., Wassen, M. J., Lammerts, E. J., and van der Heide, T.: A Global Analysis of How Human Infrastructure Squeezes Sandy Coasts, Nature Communications, 15, 432, https://doi.org/10.1038/s41467-023-44659-0, 2024.

Le Cozannet, G., Nicholls, R. J., Hinkel, J., Sweet, W. V., McInnes, K. L., Van de Wal, R. S. W., Slangen, A. B. A., Lowe, J. A., and White, K. D.: Sea Level Change and Coastal Climate Services: The Way Forward, Journal of Marine Science and Engineering, 5, 49, https://doi.org/10.3390/jmse5040049, 2017.

LeCun, Y., Bengio, Y., and Hinton, G.: Deep Learning, Nature, 521, 436–444, https://doi.org/10.1038/nature14539, 2015.

Lincke, D. and Hinkel, J.: Economically Robust Protection against 21st Century Sea-Level Rise, Global Environmental Change, 51, 67–73, https://doi.org/10.1016/j.gloenvcha.2018.05.003, 2018.

Luijendijk, A., Hagenaars, G., Ranasinghe, R., Baart, F., Donchyts, G., and Aarninkhof, S.: The State of the World's Beaches, Sci Rep, 8, 6641, https://doi.org/10.1038/s41598-018-24630-6, 2018.

Mao, Y., Harris, D. L., Xie, Z., and Phinn, S.: Global Coastal Geomorphology – Integrating Earth Observation and Geospatial Data, Remote Sensing of Environment, 278, 113 082, https://doi.org/10.1016/j.rse.2022.113082, 2022.

Masselink, G.: Introduction to Coastal Processes & Geomorphology, Routledge, Oxon [England], second edition edn., ISBN 978-1-4441-2240-4 978-0-203-78546-1 978-1-134-67291-2 978-1-134-67298-1, https://doi.org/10.4324/9780203785461, 2014.

McGranahan, G., Balk, D., and Anderson, B.: The Rising Tide: Assessing the Risks of Climate Change and Human Settlements in Low Elevation Coastal Zones, Environment and Urbanization, 19, 17–37, https://doi.org/10.1177/0956247807076960, 2007.

Moore, L. J., Hacker, S. D., Breithaupt, J., de Vries, S., Miller, T., Ruggiero, P., and Zinnert, J. C.: Ecomorphodynamics of Coastal Foredune Evolution, Nature Reviews Earth & Environment, 6, 417–432, https://doi.org/10.1038/s43017-025-00672-z, 2025.

Murray, N. J., Phinn, S. R., DeWitt, M., Ferrari, R., Johnston, R., Lyons, M. B., Clinton, N., Thau, D., and Fuller, R. A.: The Global Distribution and Trajectory of Tidal Flats, Nature, 565, 222–225, https://doi.org/10.1038/s41586-018-0805-8, 2018.

Nawarat, K., Reyns, J., Vousdoukas, M. I., Duong, T. M., Kras, E., and Ranasinghe, R.: Coastal Hardening and What It Means for the World's Sandy Beaches, Nature Communications, 15, 10 626, https://doi.org/10.1038/s41467-024-54952-1, 2024.

Nyberg, B., Gilmullina, A., Helland-Hansen, W., Nienhuis, J., and Storms, J.: Global Coastal Exposure Patterns by Coastal Type from 1950 to 2050, Cambridge Prisms: Coastal Futures, 3, e12, https://doi.org/10.1017/cft.2025.10001, 2025.

Oppenheimer, M., Glavovic, B., Hinkel, J., van de Wal, R., Magnan, A. K., Abd-Elgawad, A., Cai, R., Cifuentes-Jara, M., Deconto, R. M., Ghosh, T., Hay, J., Isla, F., Marzeion, B., Meyssignac, B., and Sebesvari, Z.: Sea Level Rise and Implications for Low Lying Islands, Coasts and Communities, 2019.

Paszke, A., Gross, S., Massa, F., Lerer, A., Bradbury, J., Chanan, G., Killeen, T., Lin, Z., Gimelshein, N., Antiga, L., Desmaison, A., Kopf, A., Yang, E., DeVito, Z., Raison, M., Tejani, A., Chilamkurthy, S., Steiner, B., Fang, L., Bai, J., and Chintala, S.: PyTorch: An Imperative Style, High-Performance Deep Learning Library, in: Advances in Neural Information Processing Systems 32, edited by Wallach, H., Larochelle, H., Beygelzimer, A., d' Alché-Buc, F., Fox, E., and Garnett, R., pp. 8024–8035, Curran Associates, Inc., 2019.

Pronk, M., Hooijer, A., Eilander, D., Haag, A., de Jong, T., Vousdoukas, M., Vernimmen, R., Ledoux, H., and Eleveld, M.: DeltaDTM: A Global Coastal Digital Terrain Model, Scientific Data, 11, 273, https://doi.org/10.1038/s41597-024-03091-9, 2024.

Raasveldt, M. and Mühleisen, H.: DuckDB: An Embeddable Analytical Database, in: Proceedings of the 2019 International Conference on Management of Data, SIGMOD '19, pp. 1981–1984, Association for Computing Machinery, New York, NY, USA, ISBN 978-1-4503-5643-5, https://doi.org/10.1145/3299869.3320212, 2019.

Rocklin, M.: Dask: Parallel Computation with Blocked Algorithms and Task Scheduling, in: Proceedings of the 14th Python in Science Conference, vol. 130, p. 136, Citeseer, 2015.

Ruder, S.: An Overview of Multi-Task Learning in Deep Neural Networks, https://doi.org/10.48550/arXiv.1706.05098, 2017.

Salman, A., Lombardo, S., and Doody, P.: Living with Coastal Erosion in Europe: Sediment and Space for Sustainability, Eurosion project reports, 2004.

Schuerch, M., Spencer, T., Temmerman, S., Kirwan, M. L., Wolff, C., Lincke, D., McOwen, C. J., Pickering, M. D., Reef, R., Vafeidis, A. T., Hinkel, J., Nicholls, R. J., and Brown, S.: Future Response of Global Coastal Wetlands to Sea-Level Rise, Nature, 561, 231–234, https://doi.org/10.1038/s41586-018-0476-5, 2018.

Sharples, C., Mount, R., Pedersen, T., Lacey, M., Newton, J., Jaskierniak, D., and Wallace, L.: The Australian Coastal Smartline Geomorphic and Stability Map Version 1: Project Report, Prepared for Geoscience Australia and the Department of Climate Change by the School of Geography and Environmental Studies, University of Tasmania, Hobart, 2009.

Small, C. and Nicholls, R. J.: A Global Analysis of Human Settlement in Coastal Zones, Journal of Coastal Research, 19, 584–599, 2003.

Stive, M. J., Aarninkhof, S. G., Hamm, L., Hanson, H., Larson, M., Wijnberg, K. M., Nicholls, R. J., and Capobianco, M.: Variability of Shore and Shoreline Evolution, Coastal Engineering, 47, 211–235, https://doi.org/10.1016/S0378-3839(02)00126-6, 2002.

Vafeidis, A. T., Nicholls, R. J., McFadden, L., Tol, R. S. J., Hinkel, J., Spencer, T., Grashoff, P. S., Boot, G., and Klein, R. J. T.: A New Global Coastal Database for Impact and Vulnerability Analysis to Sea-Level Rise, Journal of Coastal Research, 244, 917–924, https://doi.org/10.2112/06-0725.1, 2008.

Vitousek, S., Barnard, P. L., and Limber, P.: Can Beaches Survive Climate Change?, Journal of Geophysical Research: Earth Surface, 122, 1060–1067, https://doi.org/10.1002/2017JF004308, 2017.

Vitousek, S., Buscombe, D., Vos, K., Barnard, P. L., Ritchie, A., and Warrick, J.: The Future of Coastal Monitoring through Satellite Remote Sensing, Cambridge Prisms: Coastal Futures, pp. 1–43, https://doi.org/10.1017/cft.2022.4, 2022.

Woodroffe, C. D.: Coasts: Form, Process and Evolution, Cambridge University Press, 2002.

Wulder, M. A., Masek, J. G., Cohen, W. B., Loveland, T. R., and Woodcock, C. E.: Opening the Archive: How Free Data Has Enabled the Science and Monitoring Promise of Landsat, Remote Sensing of Environment, 122, 2–10, https://doi.org/10.1016/j.rse.2012.01.010, 2012.

Young, A. P. and Carilli, J. E.: Global Distribution of Coastal Cliffs, Earth Surface Processes and Landforms, 44, 1309–1316, https://doi.org/10.1002/esp.4574, 2019.